

NASA TECHNICAL
MEMORANDUM

NASA TM X-53486

1965

NASA TM X-53486

GPO PRICE \$ _____

CFSTI PRICE(S) \$ _____

Hard copy (HC) 2.00

Microfiche (MF) .50

ff 653 July 65

RESEARCH ACHIEVEMENTS REVIEW
SERIES NO. 9

RESEARCH AND DEVELOPMENT OPERATIONS
GEORGE C. MARSHALL SPACE FLIGHT CENTER
HUNTSVILLE, ALABAMA

FACILITY FORM 802

N66 34346 N66 34349
(ACCESSION NUMBER)

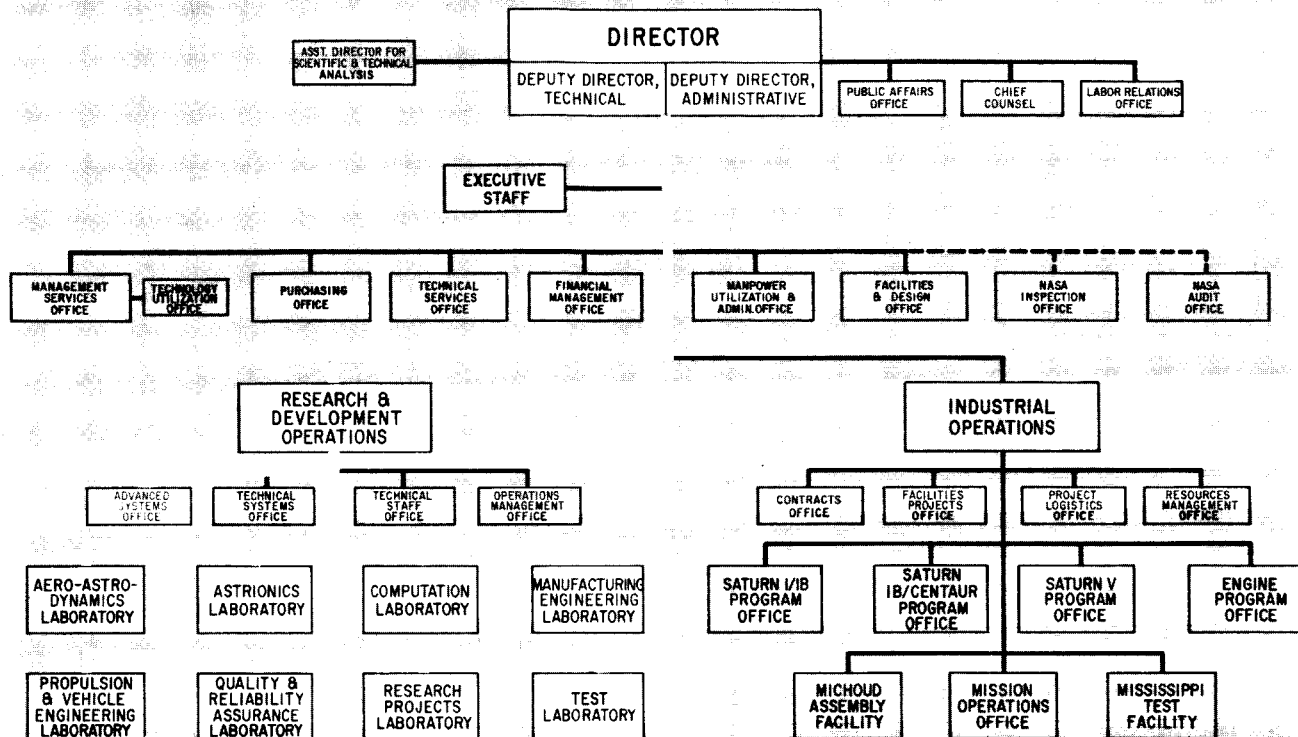
48
(PAGES)

1
(CODE)

23
(CATEGORY)

TMX-53486
(NASA CR OR TMX OR AD NUMBER)

GEORGE C. MARSHALL SPACE FLIGHT CENTER



RESEARCH ACHIEVEMENTS REVIEW SERIES INCLUDES THE FOLLOWING FIELDS OF RESEARCH

1. Radiation Physics
2. Thermophysics
3. Chemical Propulsion
4. Cryogenic Technology
5. Electronics
6. Control Systems
7. Materials
8. Manufacturing
9. Ground Testing
10. Quality Assurance and Checkout
11. Environmental and Aerodynamics
12. Atmospheric Dynamics
13. Instrumentation
14. Power Systems
15. Guidance Concepts
16. Astrodynamics
17. Advanced Tracking Systems
18. Communication Systems
19. Structures
20. Mathematics and Computation
21. Advanced Propulsion
22. Lunar and Meteoroid Physics

NASA TM X-53486

NATIONAL AERONAUTICS AND SPACE ADMINISTRATION
WASHINGTON, D. C.

GROUND TESTING AT MSFC

RESEARCH ACHIEVEMENTS REVIEW
SERIES NO. 9

RESEARCH AND DEVELOPMENT OPERATIONS
GEORGE C. MARSHALL SPACE FLIGHT CENTER
HUNTSVILLE, ALABAMA

1965

PREFACE

In 1955, the team which has become the Marshall Space Flight Center (MSFC) began to organize a research program within its various laboratories and offices. The purpose of the program was two-fold: first, to support existing development projects by research studies and second, to prepare future development projects by advancing the state of the art of rockets and space flight. Funding for this program came from the Army, Air Force, and Advanced Research Projects Agency. The effort during the first year was modest and involved relatively few tasks. The communication of results was, therefore, comparatively easy.

Today, more than ten years later, the two-fold purpose of MSFC's research program remains unchanged, although funding now comes from NASA Program Offices. The present yearly effort represents major amounts of money and hundreds of tasks. The greater portion of the money goes to industry and universities for research contracts. However, a substantial research effort is conducted in house at the Marshall Center by all of the laboratories. The communication of the results from this impressive research program has become a serious problem by virtue of its very voluminous technical and scientific content.

The Research Projects Laboratory, which is the group responsible for management of the consolidated research program for the Center, initiated a plan to give better visibility to the achievements of research at Marshall in a form that would be more readily usable by specialists, by systems engineers, and by NASA Program Offices for management purposes.

This plan has taken the form of frequent Research Achievements Reviews, with each review covering one or two fields of research. These verbal reviews are documented in the Research Achievements Review Series.

Ernst Stuhlinger
Director, Research Projects Laboratory

These papers presented June 24, 1965

ANALYSIS OF EMPIRICAL SOUND FIELDS ✓

by Gerhard H. R. Reisig

SUMMARY	1
I. INTRODUCTION	1
II. ROUTINE SOUND-FIELD AND METEOROLOGICAL MEASUREMENTS AT MISSISSIPPI TEST FACILITY	2
III. STATISTICAL EVALUATION OF MTF SOUND-FIELD DATA FOR THE YEAR 1963	3
A. Empirical Excess Sound Attenuation at MTF	5
B. Extremes of Sound Amplification	6
C. Classification of Sound-Velocity Profile Types	7
D. Probability and Directionality of Sound Focusing	9
E. Measurements of Nonstationary Sound Propagation	11
IV. CONCLUSIONS	14
REFERENCES	14

LIST OF ILLUSTRATIONS

Figure	Page
1. Orientation of Mississippi Test Facility (MTF), with Acoustic Sounding Azimuths	2
2. Acoustic Sounding Station at MTF	3
3. Meteorological Sounding Station at MTF	3
4. Number of Sound Observations Along Selected Azimuths; MTF, 1963	4
5. Polar Distribution of Average Sound Attenuation; MTF, Spring 1963	4
6. Polar Distribution of Average Sound Attenuation; MTF, Autumn 1963	4
7. Distance Function of Average Sound Attenuation (root mean square); MTF, Spring 1963	5
8. Distance Function of Average Sound Attenuation (root mean square); MTF, Autumn 1963	6
9. Components of Expected Atmospheric Sound Attenuation	7
10. Distance Function of Expected Physical Sound Attenuation	8
11. Average Deviation of Empirical Sound Attenuation from Expected Values, 40 Hz; MTF, Spring 1963	8
12. Average Deviation of Empirical Sound Attenuation from Expected Values, 160 Hz; MTF, Spring 1963	9

CONTENTS (Continued) . . .

Figure	Page
13. Sound Diffraction and Scattering in Atmosphere	9
14. Three-Sigma Negative Attenuation Deviation, 40 Hz; MTF, Spring 1963	10
15. Three-Sigma Negative Attenuation Deviation, 160 Hz; MTF, Autumn 1963	10
16. Selected Types of Characteristic Sound-Velocity Profiles	11
17. Probability of Azimuth Coverage of Sound Focusing; MSFC and MTF	11
18. Probability of Sound Focusing, by Azimuth; MTF	12
19. Probability of Sound Focusing, by Azimuth; MSFC	12
20. Comparison of Winter Sound-Focusing Probabilities, by Azimuth; MTF and MSFC	13
21. A Sound-Fluctuation Measuring Station; MTF	13
22. Microphone Catwalk for Sound-Fluctuation Measuring Field; MTF	13
23. Microphone Screening for Sound-Fluctuation Measuring Field; MTF	14
24. Sound Intensity Spatial Inhomogeneities and Temporal Fluctuations; MTF	14

RESEARCH AND DEVELOPMENT IN INSTRUMENTATION
FOR STATIC TESTING

by Albert E. Schuler

SUMMARY	15
I. INTRODUCTION	15
II. DENSITY MEASUREMENTS OF CRYOGENIC FUELS	16
III. FLOWMETERS	17
IV. LIQUID-LEVEL INSTRUMENTS	21
V. TEMPERATURE-MEASURING INSTRUMENTATION	22
VI. DAMPED ACCELEROMETERS AND ACCELEROMETER CALIBRATION SYSTEMS	23
VII. DIGITAL TRANSDUCERS	25
XIII. ULTRAHIGH-VACUUM CALIBRATION SYSTEM	26
IX. INSTRUMENTATION FOR MEASUREMENT OF OTHER EXTREME VALUES	26
X. AUTOMATIC CALIBRATION SYSTEMS	27

LIST OF ILLUSTRATIONS

Figure	Page
1. Density Measurement of Cryogenic Fuel in a Tank	16
2. Density Measurement of Cryogenic Fuel at a Point within the Tank	17
3. Density Measurement of LH ₂ in a Pipe, Using Split X-Ray Beam	17
4. LH ₂ Flowmeter Calibration Stand	18
5. Gyroscopic Mass Flowmeter (Decker)	18
6. Twin-Turbine Mass Flowmeter (Potter)	19
7. Angular Momentum Mass Flowmeter (GE)	19
8. Constant-Torque Mass Flowmeter (Waugh)	20
9. Inferential Mass Flowmeter (Quantum Dynamics)	20
10. Capacitive Mass Flowmeter (Bendix)	21
11. Capacitive and Conductive Discrete Liquid-Level Sensors	21
12. Optical Discrete Liquid-Level Sensor	22
13. Slingshot Thermocouple	23
14. Damped Accelerometer	23
15. Frequency Characteristics of Damped Accelerometer	24
16. Accelerometer Calibration System	24
17. Portable Accelerometer Calibrator	24
18. Digital Pressure Transducer	25
19. Ultrahigh-Vacuum Calibration System	26
20. Automatic Pressure Calibration System	27

LIST OF TABLES

Table	Page
I. Repeatability of Mass Flowmeter During Calibration with Liquid Hydrogen	19
II. Repeatability of Commercial Discrete Liquid-Level Sensors in Different Liquids	22

V
**SOUND SUPPRESSION TECHNOLOGY RESEARCH AT MARSHALL
 SPACE FLIGHT CENTER**

by Fritz Kramer

SUMMARY	29
I. INTRODUCTION	29
II. EARLY MODEL TESTS	29
III. LATER TEST SERIES (1962 Through Summer 1965)	31
IV. INTERMEDIATE PROTOTYPE H-1	34
V. MODELS OF SATURN V DESIGN	35
VI. CONCLUSIONS	36
REFERENCE	36

LIST OF ILLUSTRATIONS

Figure	Page
1. Velocity Distribution in Rocket Exhaust at Sea Level	30
2. Temperature Distribution in Rocket Exhaust at Sea Level	31
3. Sound Spectra at 15 Kilometers	32
4. Sound Power Level as a Function of Exhaust Velocity	33
5. Acoustical Performance of Sound-Suppression Device	34
6. Acoustical Performance of a Sound-Suppressor Model	35
7. Comparison of Acoustical Performance of Two Sound Suppressors	36

LIST OF TABLES

Table	Page
I. Gas Temperature Behind Shock Wave	30
II. Maximum Sound Suppression Obtainable as a Function of the Residual Sound Power	34

ANALYSIS OF EMPIRICAL SOUND FIELDS

By

Gerhard H. R. Reisig

SUMMARY

The large-scale field collection of acoustic data and their analysis are described in this review. The entire sound-field program has the purpose of solving complex problems of excessive noise propagation associated with the static test firing of large space-booster powerplants.

The site of data collection has been Mississippi Test Facility (MTF), where far-field sound-propagation and correlated meteorological measurements were initiated in 1962.

The statistical evaluation of sound-measurement data shows that the polar distribution of sound in the springtime (at MTF) is determined mainly by the temperature field of the atmosphere. Greater deformation of sound-intensity polar distribution occurs in the autumn as a result of the influence of the wind field.

The data on sound attenuation as a function of distance from its source revealed attenuation in excess of the expected magnitude. The excess was mainly between 1 and 10 kilometers from the source, with maximum attenuation (17 to 18 decibels) near 6 kilometers. Excess sound attenuation was compared with calculated sound dispersion. For all sound frequencies in all seasons the deviation between reference and empirical attenuation values formed a bell-shaped distribution on a semilogarithmic plot. The physical causes for the sound-attenuation behavior are considered to be atmospheric diffraction and scattering effects.

Statistical analysis of sound-intensity extremes indicated amplification of the sound signals by focusing which could be expected along selected azimuths. Empirical amplification values showed the maximum occurring in winter (50 decibels at 22 kilometers).

For the analysis of correlation between empirical sound data and local atmospheric sound-propagation conditions, the concept of analytical classification of sound-velocity profiles has been developed. Examination of over a quarter-million individual sound-velocity profiles indicates that 33 profile types for heights up to 3 kilometers constitute

the empirical possibilities of sound-propagation conditions in southeastern United States.

Since the focusing qualities of each sound-velocity profile can be determined as a class characteristic, the overall probabilities of focusing occurrence can be obtained. The severity of focusing, as based upon lateral spread of focusing areas, has been determined. The data for MTF indicate focusing is most severe in winter, with the direction toward east being most affected.

Sound propagation is a fluctuating phenomenon because atmospheric conditions vary continuously. A measuring system for analyzing the nonstationary sound-propagation phenomena has been established. The analysis of the acoustic fluctuation data is supposed to provide "dynamic" perturbation functions of sound, which are to be superimposed on the related characteristic sound-velocity-profile type.

The ultimate result of the program will be the establishment of reliable contingency tables showing the relationship between atmospheric parameters and far-field sound intensities. These data will be the basis for more accurate sound-propagation forecasting for static firing tests.

I. INTRODUCTION

Associated with static test firing of large space-booster powerplants are complex problems in noise generation and propagation. Current knowledge of the acoustical behavior of the atmosphere is insufficient for an analytical treatment of the problems of excessive noise propagation. Therefore, these problems require evaluation and analysis of information which must be obtained empirically, and on the largest practicable scale.

It was necessary to have an operational guide for test-noise monitoring available at the time the Mississippi Test Facility (MTF) was activated. The Mississippi Test Site (MTS), therefore, was selected for the collection of statistical data on far-field sound propagation. Routine sound-propagation and meteorological measurements were begun at MTS in late 1962. Work since that time has included

a statistical evaluation of MTF sound-field data of the year 1963 in terms of an analysis of the excessive sound attenuation; an appraisal of the sound amplification; the classification of sound-velocity profile types; an analysis of the probability of sound focusing with regard to season, azimuth, and directionality; and the development of a measuring system to detect and analyze the nonstationary properties of atmospheric sound propagation.

The goal of the extensive acoustic measuring program at MTF is the provision of comprehensive and reliable contingency tables for the relationships between atmospheric parameters and far-field sound intensities. These tables are a basic prerequisite for high-confidence sound-propagation forecasting for static rocket-firing tests.

II. ROUTINE SOUND-FIELD AND METEOROLOGICAL MEASUREMENTS AT MISSISSIPPI TEST FACILITY

In late 1962, both an acoustical and a meteorological sound station were activated at the Mississippi Test Site near Gainesville, Mississippi (Fig. 1).

Eight azimuths around the wind rose were selected for routine sound-propagation measurements. (The azimuths were 30, 76, 103, 140, 175, 232, 280, and 342 degrees.) One series of measurements was made at least each morning and afternoon, 7 days a week. The sound to be monitored was generated by a pneumatic horn of about 5000 acoustic

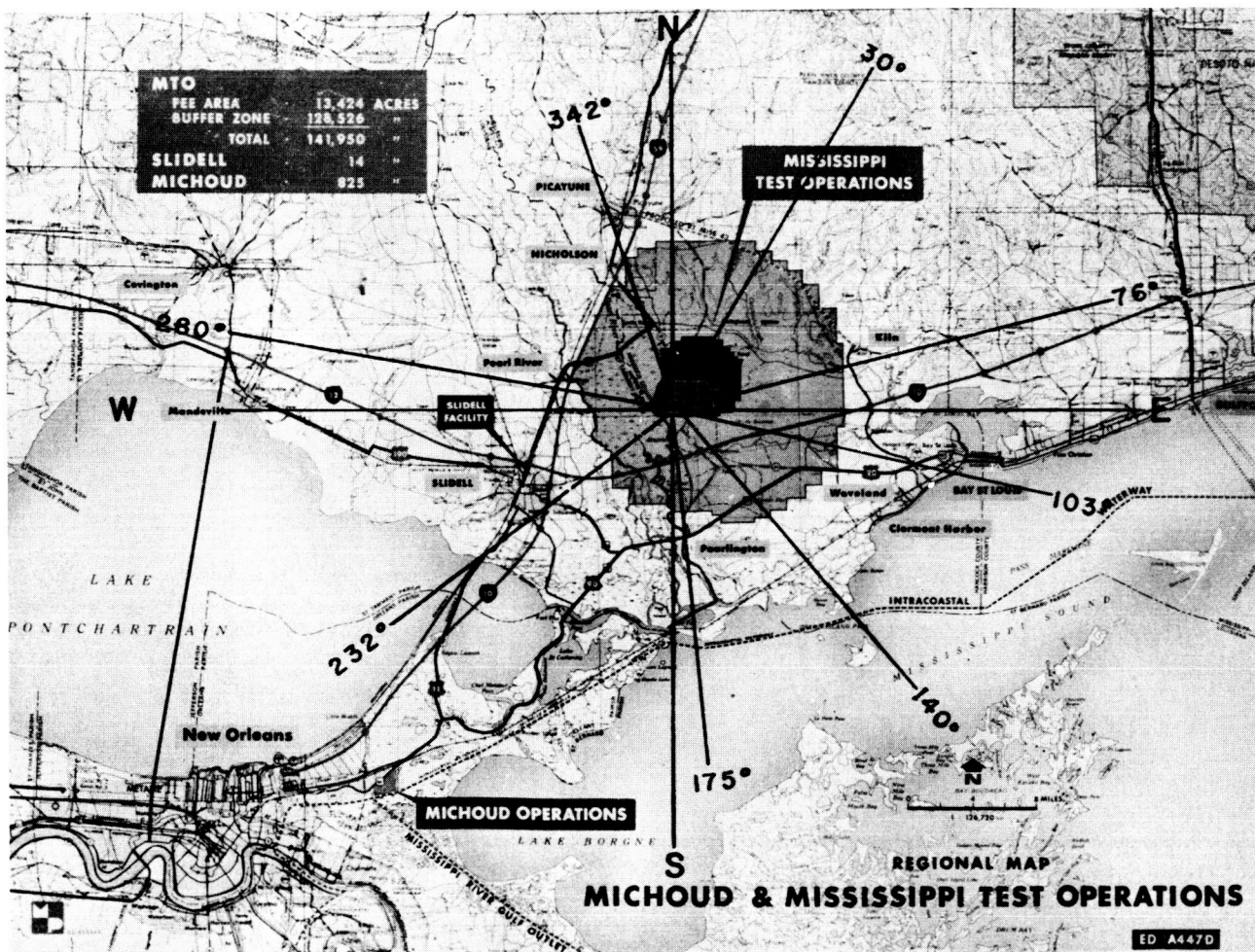


FIGURE 1. ORIENTATION OF MISSISSIPPI TEST FACILITY (MTF), WITH ACOUSTIC SOUNDING AZIMUTHS

watts power, which transmitted four discrete low frequencies (40, 80, 120, and 160 Hz) and a spectrum of random noise (Fig. 2). Personnel with hand-carried sound-pressure-level meters for visual data gathering were dispatched along the established azimuth lines. Sound emission from the horn and acquisition of sound data were coordinated by radio communication. The horn soundings were about 10 seconds per measurement.

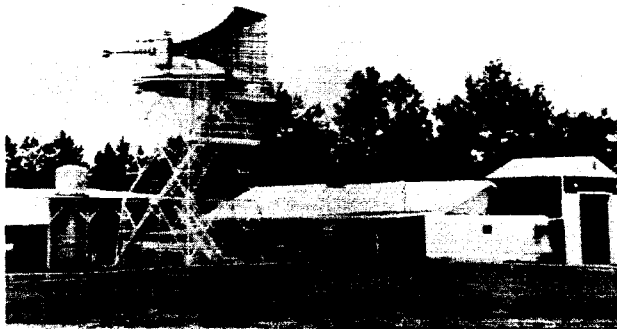


FIGURE 2. ACOUSTIC SOUNDING STATION AT MTF

To obtain the closest possible correlation between acoustic and atmospheric data, the acoustic measuring series and radiosonde ascents from the meteorological sound station (Fig. 3) were run simultaneously.

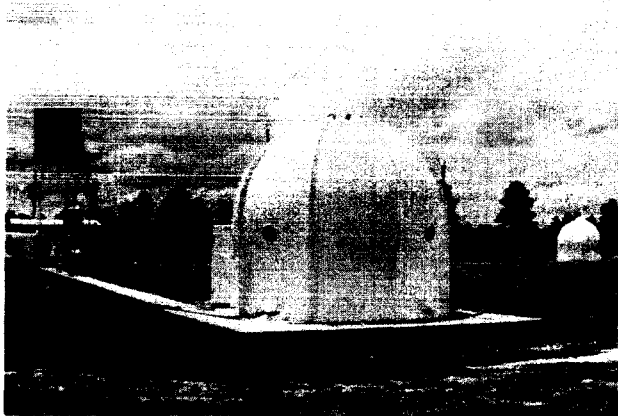


FIGURE 3. METEOROLOGICAL SOUNDING STATION AT MTF

III. STATISTICAL EVALUATION OF MTF SOUND-FIELD DATA FOR THE YEAR 1963

The first phase of the statistical analysis of atmospheric sound propagation was concerned with the evaluation of the MTF acoustic data population for 1963. Twenty-five measuring locations were selected along each of the specified azimuth directions. If each of the 25 stations had contributed a complete set of useful data for each measuring series, each azimuth would have provided 5921 sound pressure level (SPL) measurements for the year. The series was incomplete, however, because of a number of adverse conditions. The chief ones were temporary inaccessibility of the measuring locations because of poor ground conditions, and the weakness of the horn signal because of adverse sound-propagation conditions in the atmosphere, which resulted in the predominance of background noise over the acoustical signal. The graphic presentation of the number of available observations as a function of distance (Fig. 4), for example, indicates that, at 6 kilometers, the number of actual observations dropped to about 70 percent of all possible ones, and beyond 7 kilometers it dropped to 34 percent. Because these data favored cases of atmospheric conditions leading to sound amplification, the sound data at greater distances from the source are considered biased. To improve homogeneity of the data population, measuring sequence gaps not wider than two consecutive stations were closed by linear interpolation of sound-level values.

The statistical evaluation of the 1963 sound-measuring data, based on the conditions described, revealed the following main features of the sound field at MTF.

During springtime, the polar coordinate plot of average sound attenuation shows an almost circular pattern for a 40-Hz sound frequency (Fig. 5). The numerals on the polygons of Figures 5 and 6 indicate the seasonal root-mean-square values of sound attenuation, in decibels. The polygons are drawn only for identification of locations of equal sound-intensity values. The lines between the corners of these polygons do not have any numerical meaning. A slight shift of the distances of equal sound intensity toward the east indicates the influence of western winds on the polar sound-intensity distribution. Because the wind factor is slight, this polar distribution is essentially determined by the temperature field of the atmosphere. This means that a sound-velocity profile without wind influence, and depending

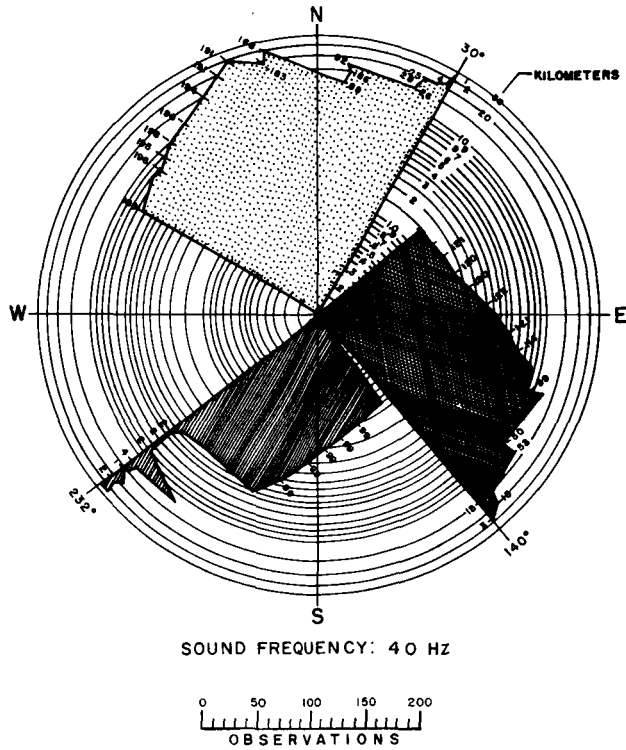


FIGURE 4. NUMBER OF SOUND OBSERVATIONS ALONG SELECTED AZIMUTHS; MTF, 1963

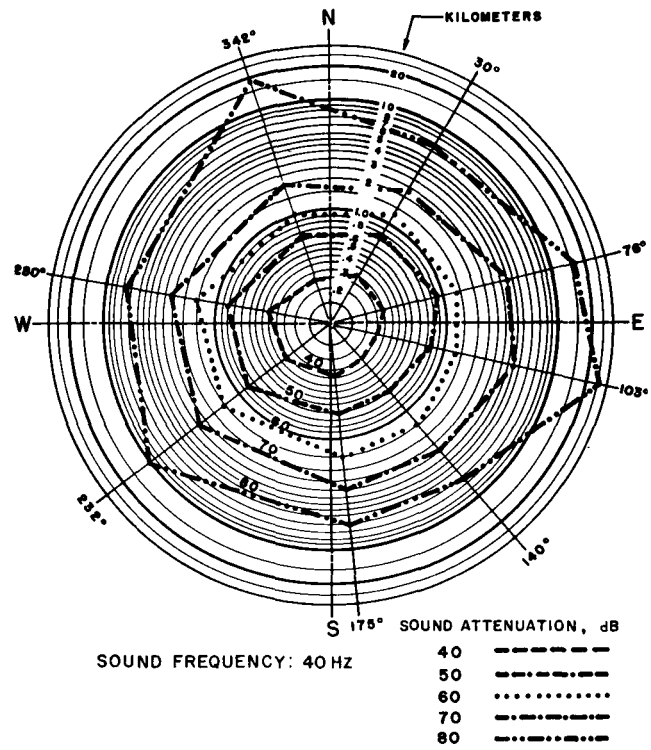


FIGURE 6. POLAR DISTRIBUTION OF AVERAGE SOUND ATTENUATION; MTF, AUTUMN 1963

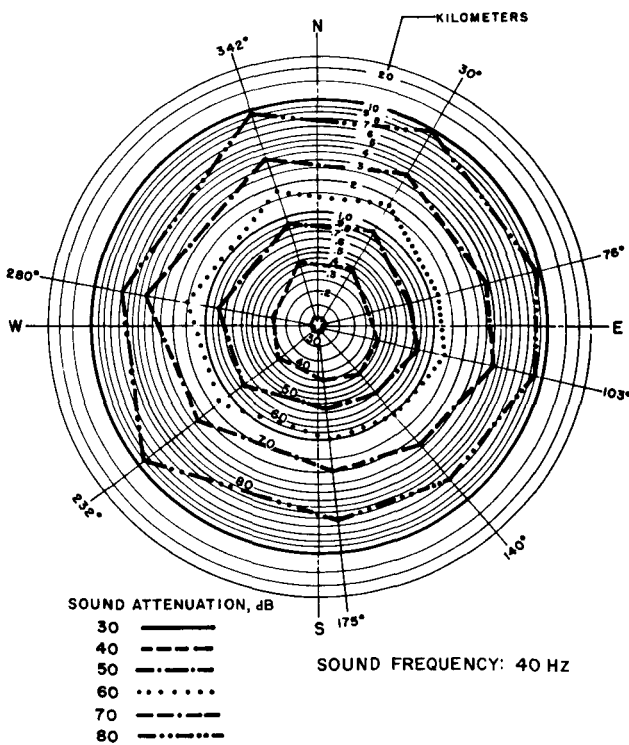


FIGURE 5. POLAR DISTRIBUTION OF AVERAGE SOUND ATTENUATION; MTF, SPRING 1963

only upon atmospheric temperature, generates identical sound-propagation conditions in any azimuth around the wind rose. A circular polar diagram of sound attenuation is produced in this case.

For the same sound frequency (40 Hz) in the autumn, there is a more pronounced deformation of the polar distribution of sound intensity. As indicated in Figure 6, deviations from the circular shape are obvious in the western, northeast, and southeast quadrants. This configuration indicates the dominance of stronger wind components from the west, northwest, and southwest over the temperature field.

The springtime average sound attenuation is presented in Figure 7 as a function of the distance from the sound source, for four selected azimuths. (The selected azimuths, 103, 175, 280, and 342 degrees, were the closest to the desired 90-degree intervals that could be obtained practicably.) For comparison, a long-short dashed straight line represents pure geometric dispersion of sound energy of spherical wave fronts (inverse square law for sound intensity); the attenuation rate is 6 decibels per octave of radial distance. The remarkable feature of this distance function of sound attenuation is the excessive attenuation between 1 and 10 kilometers from the sound source. The excessive attenuation reached a maximum at 6 kilometers (approximately), with a value about 18 decibels from the line of geometric sound dispersion.

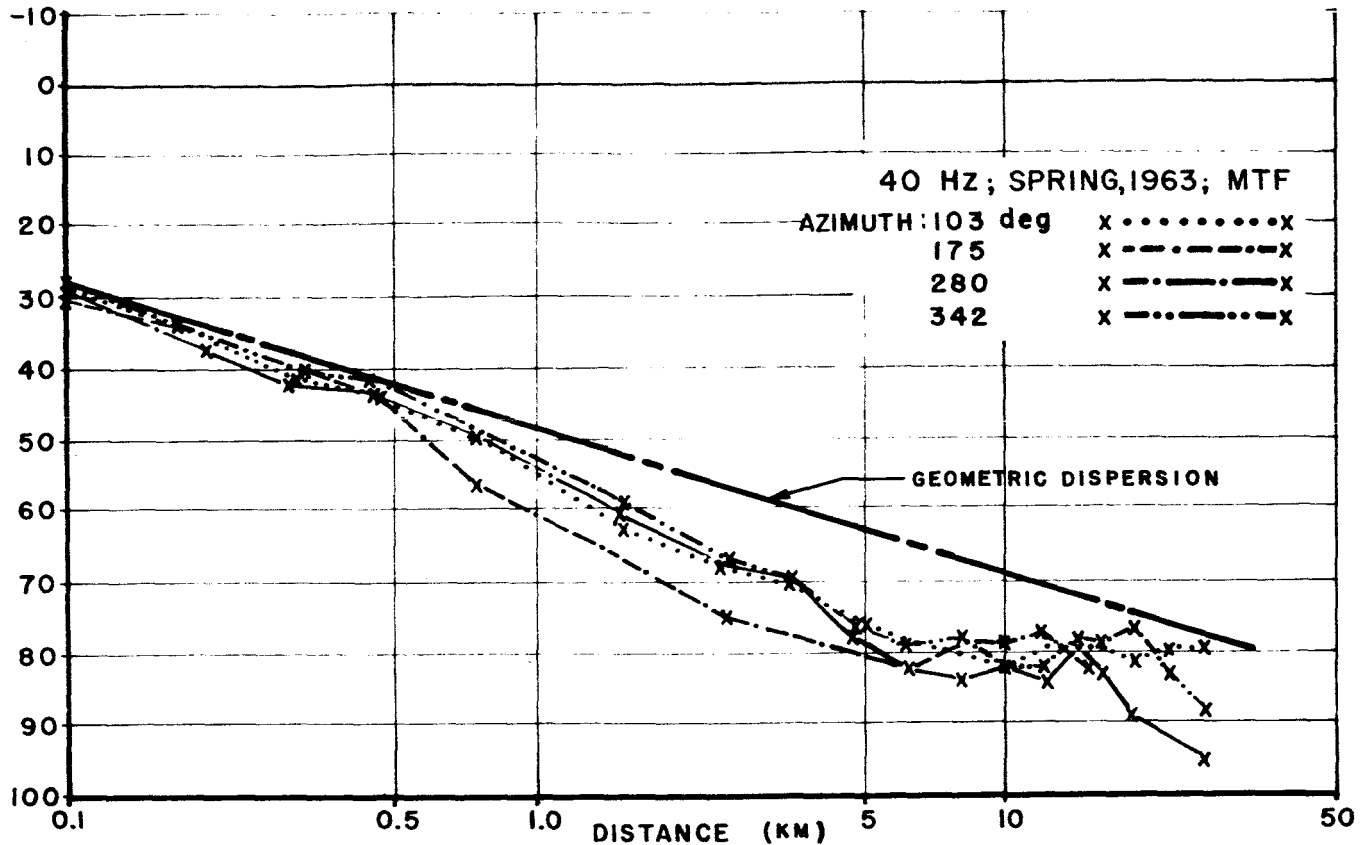


FIGURE 7. DISTANCE FUNCTION OF AVERAGE SOUND ATTENUATION (ROOT MEAN SQUARE); MTF, SPRING 1963

The distance function of sound attenuation in the autumn exhibits the same features as for spring, but is less uniform (Fig. 8). The maximum excessive attenuation also is at 6 kilometers, and its value is 17 decibels. This feature of excess attenuation proved to be typical with various excess amplitudes, for all azimuths, seasons, and sound frequencies.

A. EMPIRICAL EXCESS SOUND ATTENUATION AT MTF

The distance function of sound attenuation was compared with the expected local attenuation, so that the physical reasons for the distance-dependent excessive sound attenuation could be analyzed. The following known physical contributors to sound attenuation were taken into account (Fig. 9): (1) the classical attenuation, including air viscosity, air heat conduction, heat radiation of the atmosphere, and diffusion of the air molecules; (2) atmospheric attenuation due to molecular absorption in the air, which is a second order function of the sound frequency; and (3) a not too precisely defined amount of sound attenuation due to atmospheric scattering of sound waves.

For a sound frequency of 40 Hz, the distance function of expected sound attenuation is practically identical with the geometric sound dispersion function (Fig. 10). For a sound frequency of 160 Hz, the distance function of the expected sound attenuation gradually deviates from the geometric function; this deviation results from the quadratic dependency on frequency of the classical, molecular, and scattering attenuation (expressed as the terms B_k , B_m , and B_s , respectively, in the attenuation equation of Figure 9). Thus, at a 50-kilometer distance, the total expected attenuation increases by about 6.5 decibels above the geometric sound dispersion (the zero line).

During all seasons, in all azimuth directions, and for all sound frequencies, the deviation of average empirical sound attenuation from the expected value exhibits a typical trend in the form of a bell-shaped curve on a semilogarithmic plot (Figs. 11 and 12). The peak value of the average deviation is 21 decibels for 40 Hz (azimuth 280 degrees, summer, Fig. 11), and 24 decibels for 160 Hz (azimuth 175 degrees, spring and summer, Fig. 12). The peak signal strength for both frequencies occurs in summer.

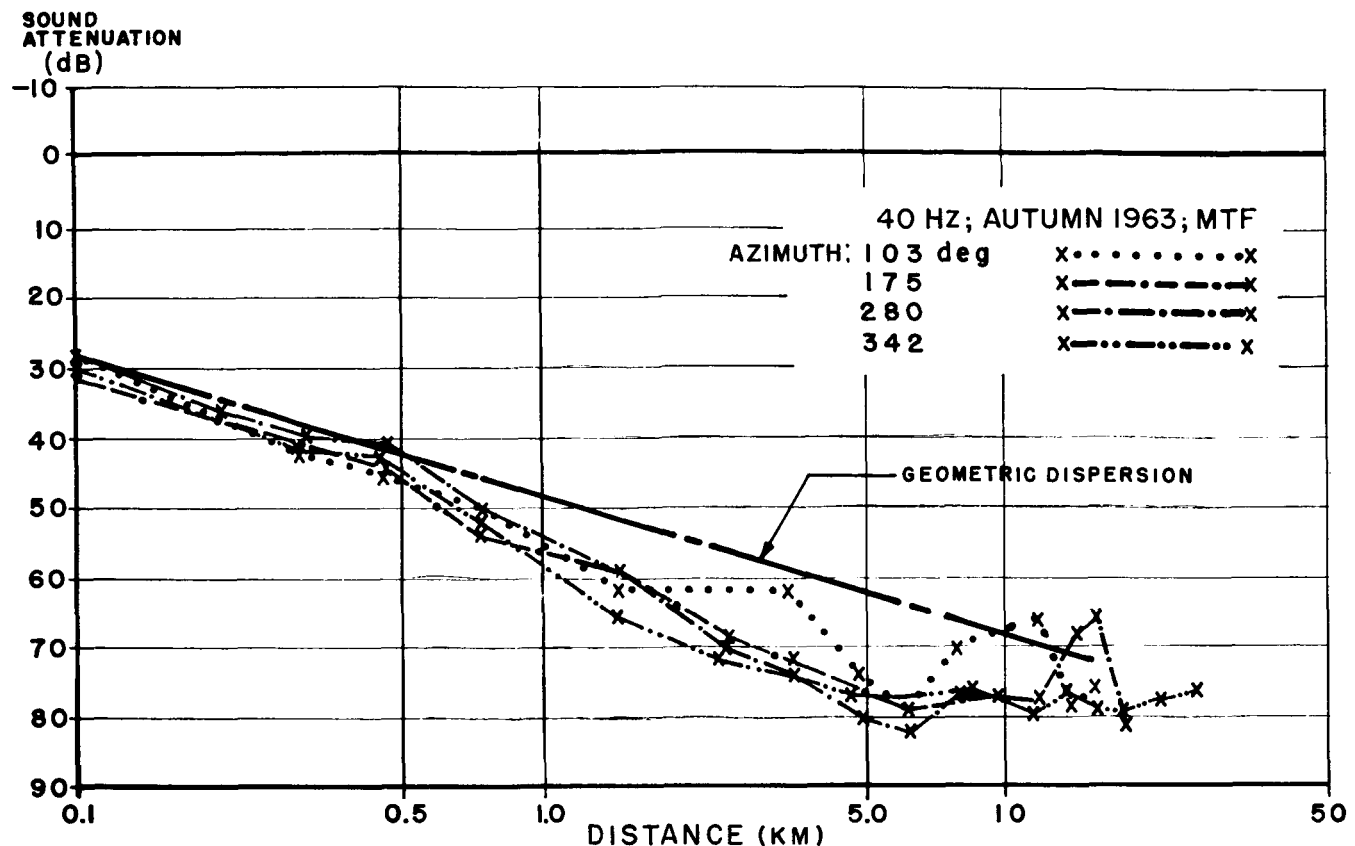


FIGURE 8. DISTANCE FUNCTION OF AVERAGE SOUND ATTENUATION (ROOT MEAN SQUARE); MTF, AUTUMN 1963

A physical explanation of this sound-attenuation phenomenon may be found in atmospheric diffraction and scattering effects (Fig. 13). The diffraction component of sound attenuation results from the negative gradients of the sound-velocity profile in the atmosphere. The negative gradients can be caused by either a negative atmospheric temperature-gradient profile or a negative wind-gradient profile, or a combination of both [1,2].

With regard to a given azimuth direction, a head wind will bend the sound rays upward, thus causing the diffractive attenuation of the sound waves, or a silent zone. However, no absolute silence has been observed in the actual sound field; the theoretically infinite attenuation is limited to a value of 24 decibels. The physical reason for the finite limit of attenuation in the silent zones is the scattering or "spilling" of sound energy into these zones. This scattering of sound is an effect of the condition of the atmosphere, which is inhomogeneous and constantly changing because of heat convection in the form of buoyant air bubbles and because of turbulence eddies generated by wind shear. Available empirical sound-field data so far are not comprehensive enough to permit a detailed analysis of the very significant

sound-scattering effect. A sound-measuring project has been initiated at MTF for collecting sound-scattering data over large distances and on a statistical scale over all seasons of the year.

An essential instrumentation problem in the sound measurement was the monitoring of the background noise, which garbled a substantial amount of the sound-measuring data at MTF for the year 1963. Hence, the question which has to be answered is whether the limit of 24-decibel sound attenuation above the expected sound attenuation is caused by the sound-propagation conditions of the atmosphere, or whether this limit possibly represents a cutoff value caused by a masking background noise.

B. EXTREMES OF SOUND AMPLIFICATION

The statistical analysis of the empirical sound-propagation data at MTF also permits an appraisal of the magnitude of the local sound amplification, particularly that caused by focusing of sound energy. The criterion selected for the analysis of extreme amplification of sound intensity during propagation through the atmosphere was the limit formed by the negative three standard deviations from the average

$$A = \log \frac{d}{d_0} + (\bar{B}_k + \bar{B}_m + \bar{B}_s) \cdot d \quad (\text{dB})$$

d = DISTANCE (km)

d_0 = 0.1 (km)

B_k = "CLASSICAL" ATTENUATION

B_m = MOLECULAR ATTENUATION

B_s = SCATTERING ATTENUATION

B_k :

$$f = 40 \text{ Hz} : B_{k40} = 2 \times 10^{-4} \quad (\text{dB/km})$$

$$80 \text{ Hz} : B_{k80} = 8 \times 10^{-4} \quad (\text{dB/km})$$

$$120 \text{ Hz} : B_{k120} = 2.0 \times 10^{-3} \quad (\text{dB/km})$$

$$160 \text{ Hz} : B_{k160} = 3.5 \times 10^{-3} \quad (\text{dB/km})$$

B_m :

$$f = 40 \text{ Hz} : B_{m40} = 3 \times 10^{-3} \quad (\text{dB/km})$$

$$80 \text{ Hz} : B_{m80} = 1.3 \times 10^{-2} \quad (\text{dB/km})$$

$$120 \text{ Hz} : B_{m120} = 3 \times 10^{-2} \quad (\text{dB/km})$$

$$160 \text{ Hz} : B_{m160} = 5 \times 10^{-2} \quad (\text{dB/km})$$

B_s :

$$f = 40 \text{ Hz} : B_{s40} = 5.5 \times 10^{-3} \quad (\text{dB/km})$$

$$80 \text{ Hz} : B_{s80} = 2 \times 10^{-2} \quad (\text{dB/km})$$

$$120 \text{ Hz} : B_{s120} = 4.0 \times 10^{-2} \quad (\text{dB/km})$$

$$160 \text{ Hz} : B_{s160} = 7.5 \times 10^{-2} \quad (\text{dB/km})$$

FIGURE 9. COMPONENTS OF EXPECTED ATMOSPHERIC SOUND ATTENUATION

attenuation deviation. This limit of three standard deviations, or "three-sigma" values, comprises 99.73 percent of all empirical sound-attenuation data obtained during the year 1963 at MTF. This three-sigma limit indicates the strength of actual sound amplification by focusing that can be expected in the large majority of cases along the selected azimuth directions.

The 40-Hz sounding frequency, as an example, shows the three-sigma sound-amplification probabilities in four azimuth directions during spring (Fig. 14). The highest sound-amplification values during this season occur at 1.5 kilometers distance, and beyond 7 kilometers. In the distance functions presented, the maximum amplitude of sound amplification amounts to about 20 decibels. However, the extreme amplification occurs during winter on the

140-degree azimuth. At 1.5 kilometers distance, it rises to 35 decibels above the expected value. At 22 kilometers distance, a peak value of almost 50 decibels amplification is reached, probably because of focusing.

The 160-Hz sounding frequency during autumn shows a maximum amplitude of 16 decibels (Fig. 15). The absolute extreme sound amplification occurs during winter and on the 140-degree azimuth (as for 40-Hz sound), with peak values of about 32 decibels above the expected attenuation at both 1.5 and 22 kilometers distance from the sound source.

C. CLASSIFICATION OF SOUND-VELOCITY PROFILE TYPES

The first physical and statistical results of the analyses of empirical sound-field data serve as a guide to the sound-propagation phenomena to be encountered at MTF. The next step in the analysis of the distance functions of observed local sound intensities calls for the closest possible correlation between empirical sound data and the local atmospheric sound-propagation conditions at the time of the acoustic observation. For this novel and intricate analysis, the vertical profile of sound velocity versus altitude was selected as the atmospheric parameter function responsible for the sound-intensity distribution in the sound field at the surface. The vertical sound-velocity profile is determined from the meteorological data of each radiosonde ascent in support of acoustic measurements.

The basic idea for the newly conceived correlation analysis consists of the classification of the vertical sound-velocity profiles into characteristic types (Fig. 16). The statistical populations of these profile types preserve the physical features which characterize each significant class of atmospheric sound-propagation conditions. Thus, the individual statistical populations of sound profiles are determined only by the structure of the atmosphere at a particular instant. Theoretically, each profile type could occur at any time, independent of a particular day, month, or season. This concept does not suppress the physical features of the profiles, as conventional statistical treatments usually do, for instance, by averaging physical quantities over arbitrary time intervals without specific physical meaning.

The method of classification of the vertical sound-velocity profiles has been developed by Essenwanger, US Army Missile Command [3]. With this method, the profiles are represented in terms of polynomials up to the sixth order. The profile representation is accomplished either by "pure" polynomials of the

SOUND ATTENUATION (dB)

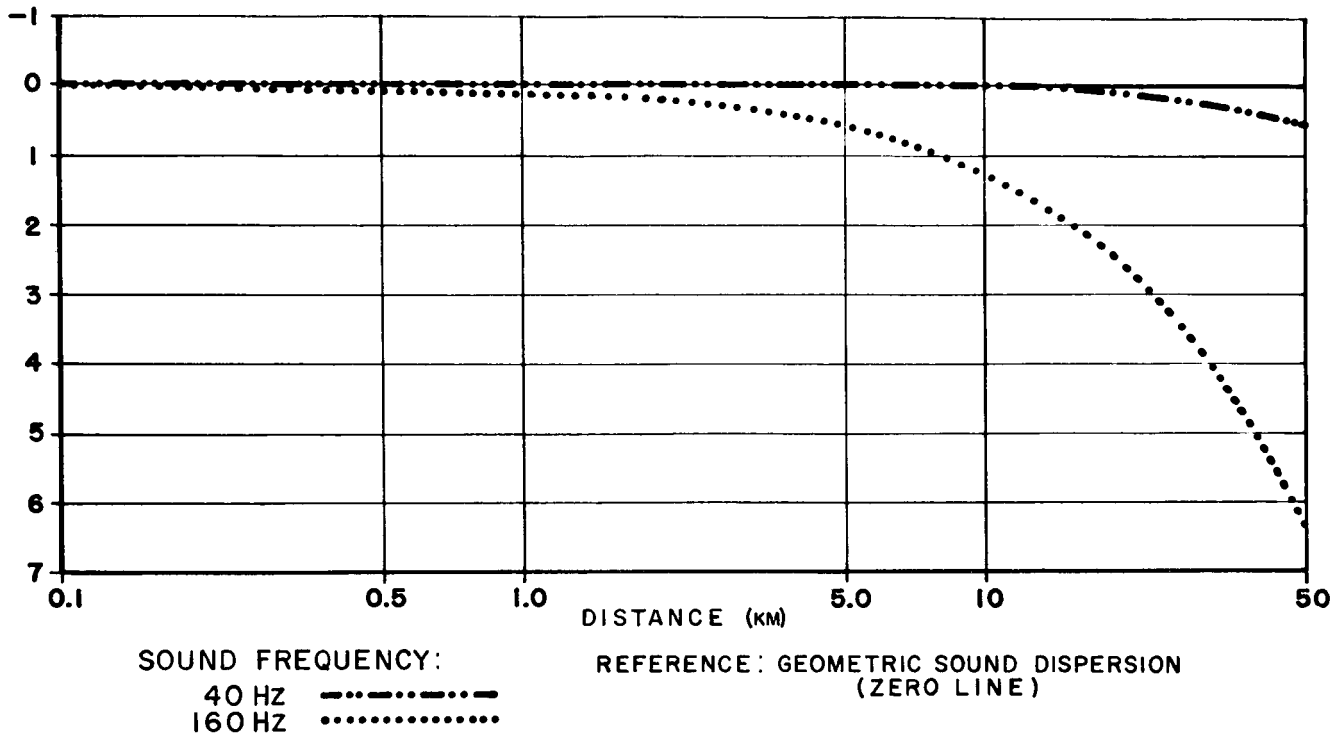


FIGURE 10. DISTANCE FUNCTION OF EXPECTED PHYSICAL SOUND ATTENUATION

SOUND ATTENUATION (dB)

EXTREME: 40 Hz; SUMMER 1963; MTF AZIMUTH 280 DEG. x-----x

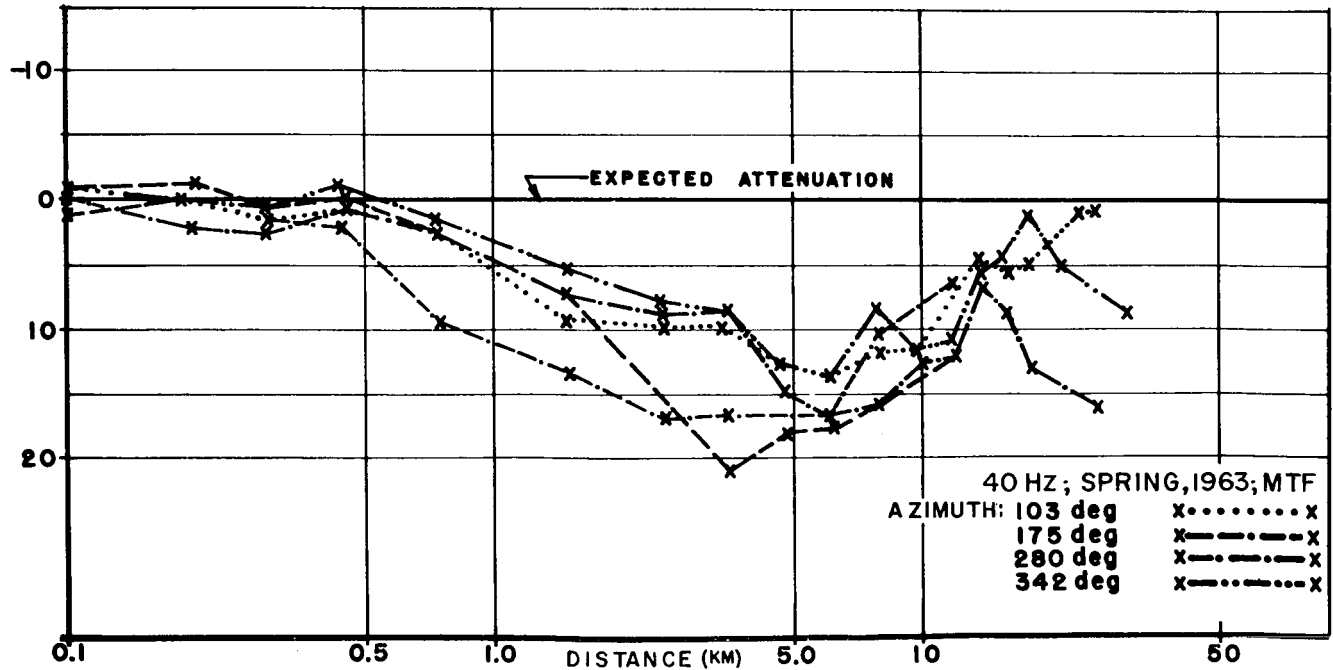


FIGURE 11. AVERAGE DEVIATION OF EMPIRICAL SOUND ATTENUATION FROM EXPECTED VALUES, 40 Hz; MTF, SPRING 1963

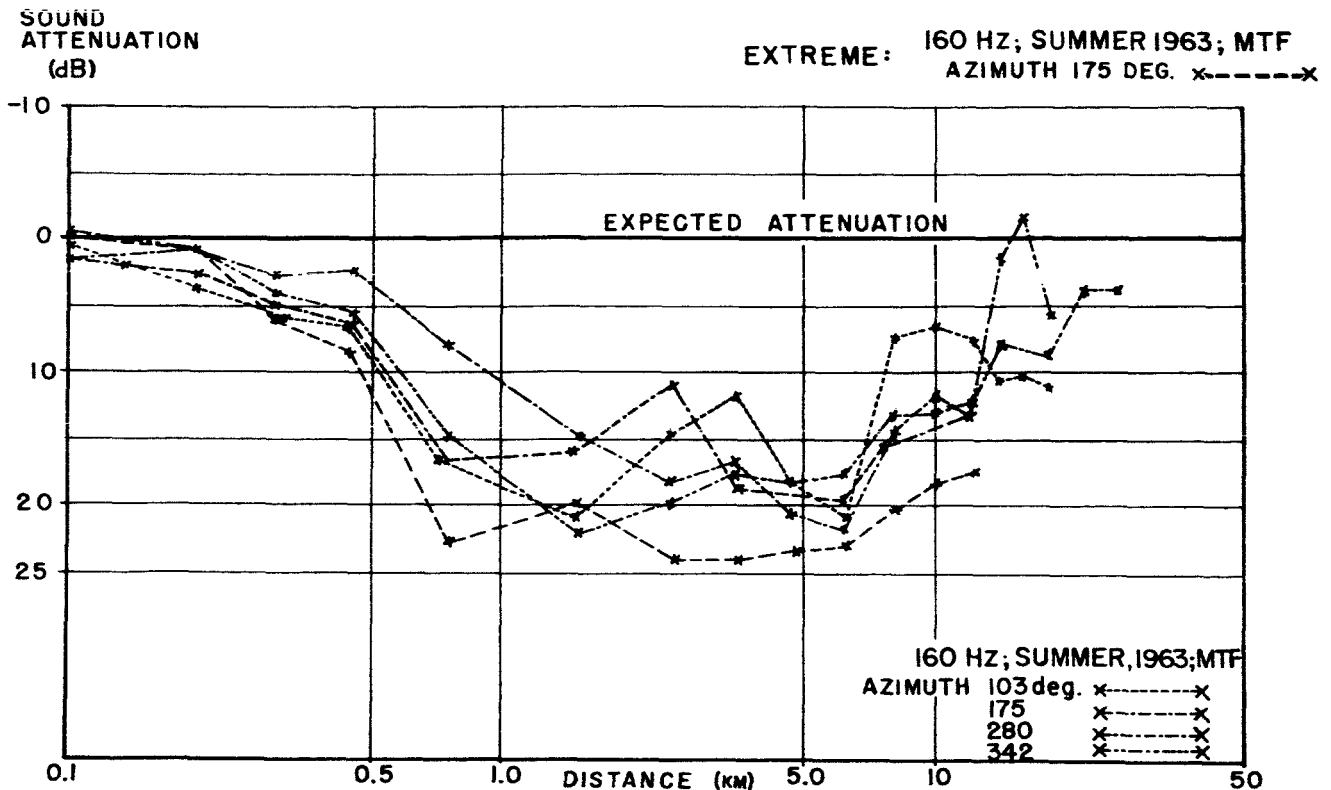


FIGURE 12. AVERAGE DEVIATION OF EMPIRICAL SOUND ATTENUATION FROM EXPECTED VALUES, 160 Hz; MTF, SPRING 1963

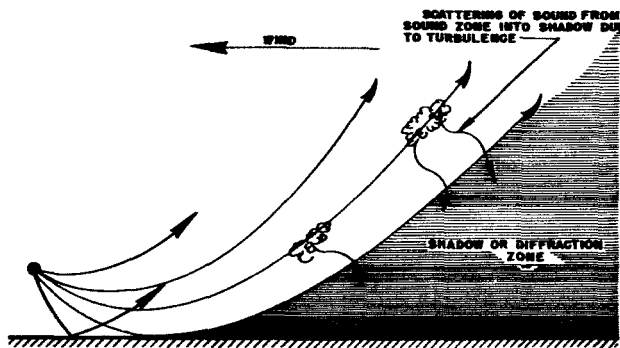


FIGURE 13. SOUND DIFFRACTION AND SCATTERING IN ATMOSPHERE

order one through six, like types 1 and 11 in Figure 16, or by a superposition of a basic polynomial of predominant weight with higher order components of lesser weight, like types 22 and 27. The analytical investigation of about 252,000 individual sound-velocity profiles of the stations at MTF, at Huntsville, Alabama (Marshall Space Flight Center), and at Nashville, Tennessee, has established that, up to a height of 3 kilometers, 33 sound-velocity profile types essentially constitute the empirical possibilities

of the sound-propagation conditions in the southeastern United States.

The quality of matching between the empirical sound-velocity profile and its analytical prototype has to result in a correlation coefficient of at least 0.7, which is a strict requirement. However, in most cases of matching of the investigated sound-velocity profiles, a correlation coefficient of 0.9 has been achieved, which is an excellent result.

Certain profile types rarely occur in their ideal form. They are sensitive to "static" perturbations of the atmospheric parameters which express themselves in higher order polynomial components of small weights. These perturbations lead to focusing properties of profile types which, according to acoustic ray theory, could not affect focal concentration of sound energy. This phenomenon explains the focusing probabilities for the profile types such as 1 and 22 in Figure 16.

D. PROBABILITY AND DIRECTIONALITY OF SOUND FOCUSING

The focusing or nonfocusing qualities of each established type of sound-velocity profile can now be

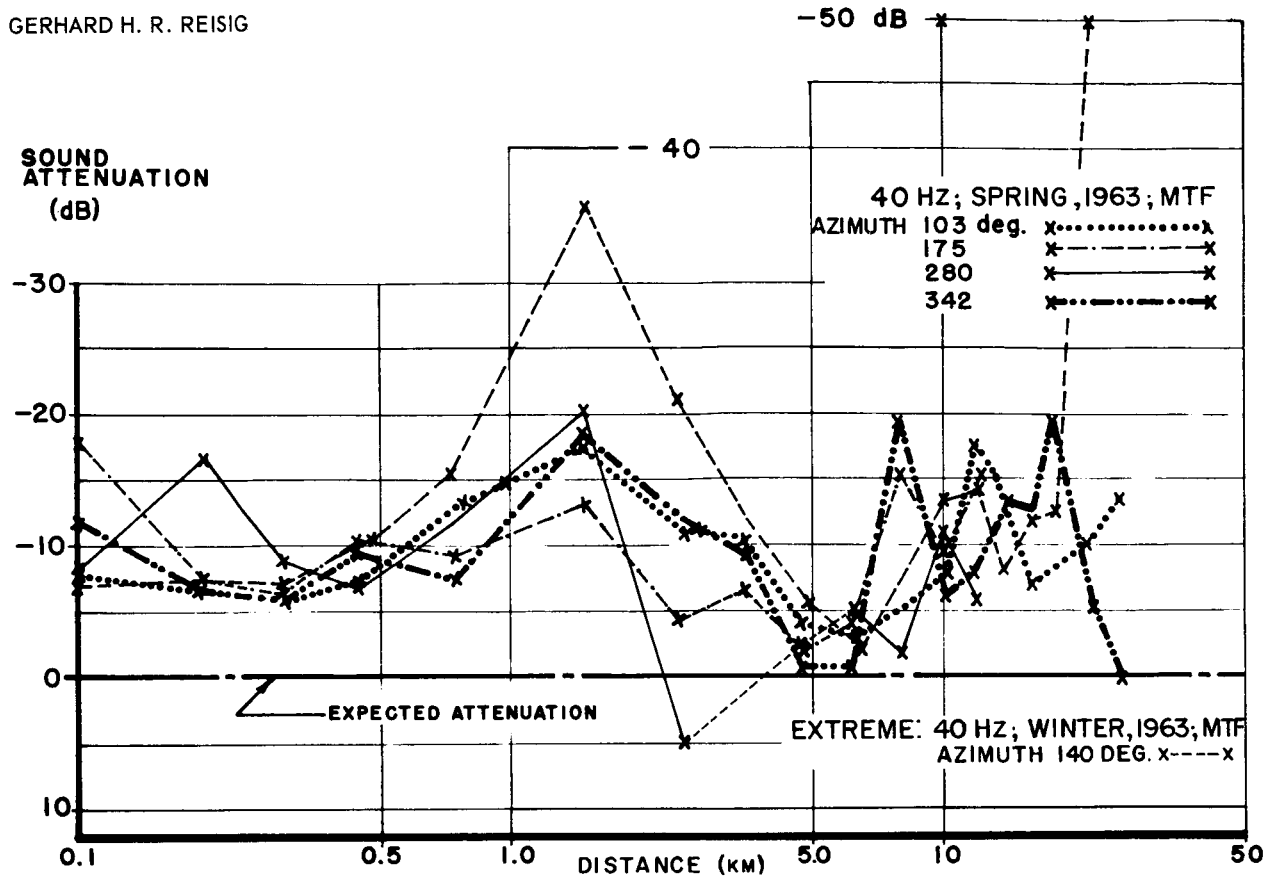


FIGURE 14. THREE-SIGMA NEGATIVE ATTENUATION DEVIATION, 40 Hz; MTF, SPRING 1963

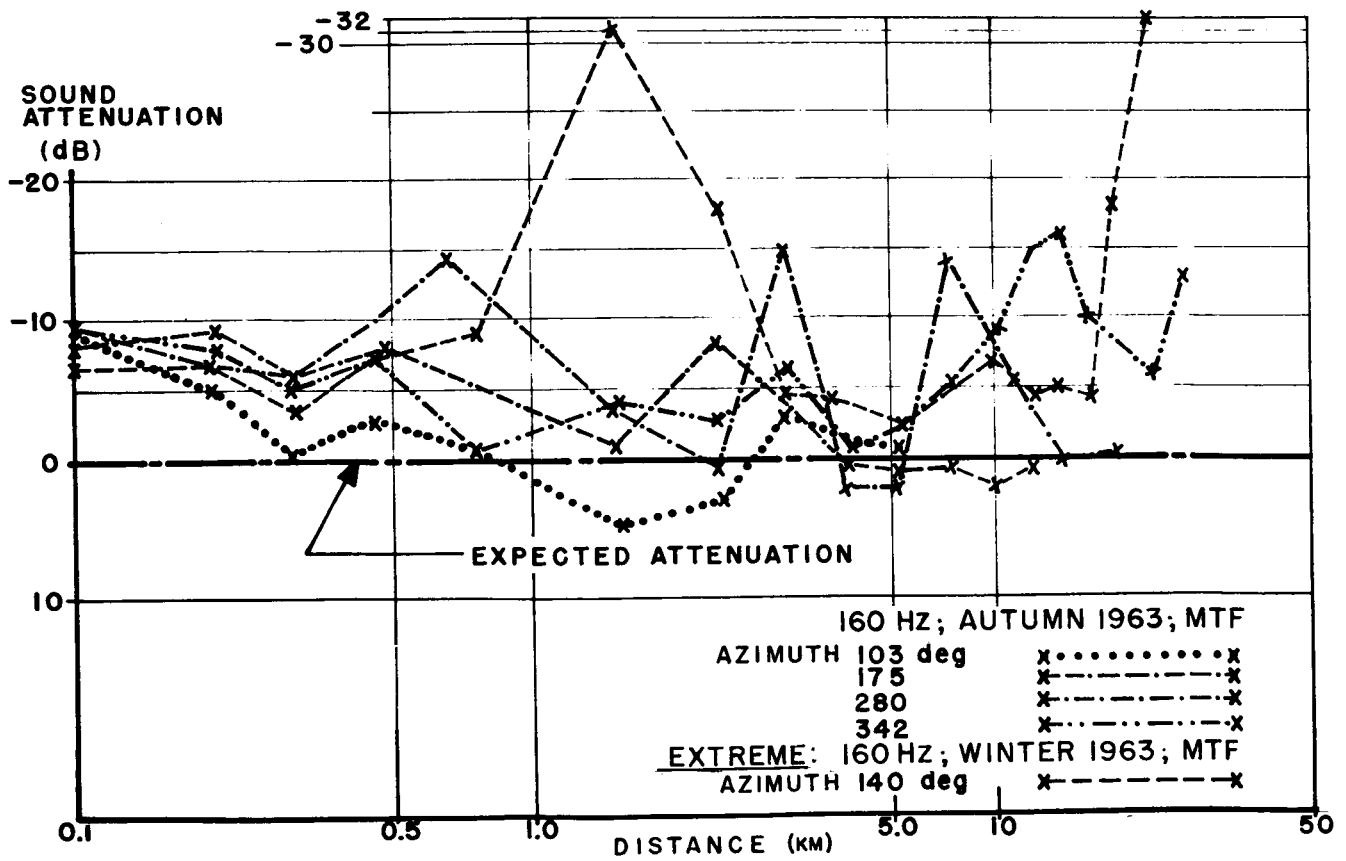


FIGURE 15. THREE-SIGMA NEGATIVE ATTENUATION DEVIATION, 160 Hz; MTF, AUTUMN 1963

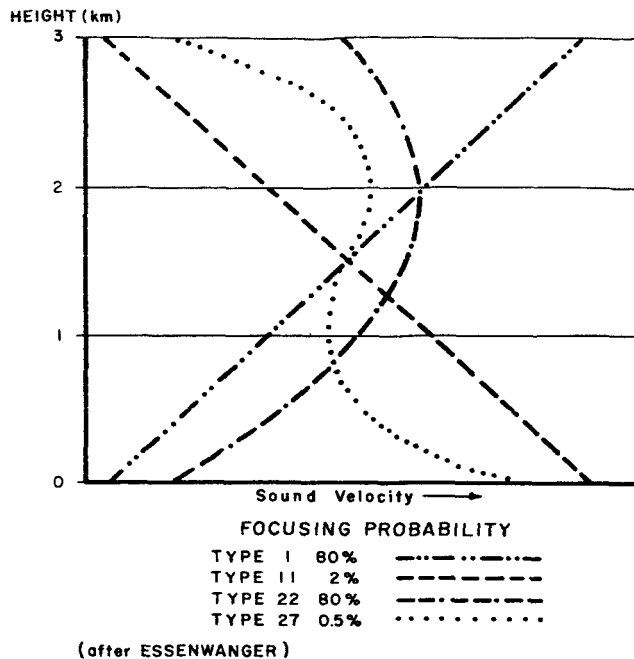


FIGURE 16. SELECTED TYPES OF CHARACTERISTIC SOUND-VELOCITY PROFILES

determined as a class characteristic. The sound-focusing properties of each empirical sound-velocity profile of the MTF and Huntsville, Alabama (MSFC), stations have been analyzed [4] with this established classification. A summary of these investigations (Fig. 17) gives the overall probabilities of focusing occurrence in the two stations, for the four seasons of the year in the afternoon (1200 to 1700 hours, local time). The favorable conditions of nonfocusing during summer are readily evident, with 72 percent nonfocusing at MTF and 76 percent at MSFC. Figure 17 also indicates the severity of focusing by expressing the lateral spread of focusing areas (directionality) covered by high-intensity sound amplification. For instance, during winter the total focusing probability at MTF is 92 percent, and for MSFC, 87 percent. In these cases, the focusing area extends over an azimuth sector of more than 90 degrees, with a probability of 58 percent at MTF and 54 percent at MSFC. During the forenoon hours, the focusing probabilities have been found even more severe because of the peculiar structure of the atmosphere. During summer, however, the focusing probability is only 28 percent at MTF and 24 percent at MSFC. The lateral spread of the focusing area in severe cases (azimuth sector over 90 degrees) occurs with a probability of only 5 percent at MTF and 9 percent at MSFC.

For rocket-firing tests, it is essential to know which areas around the test facility will be most

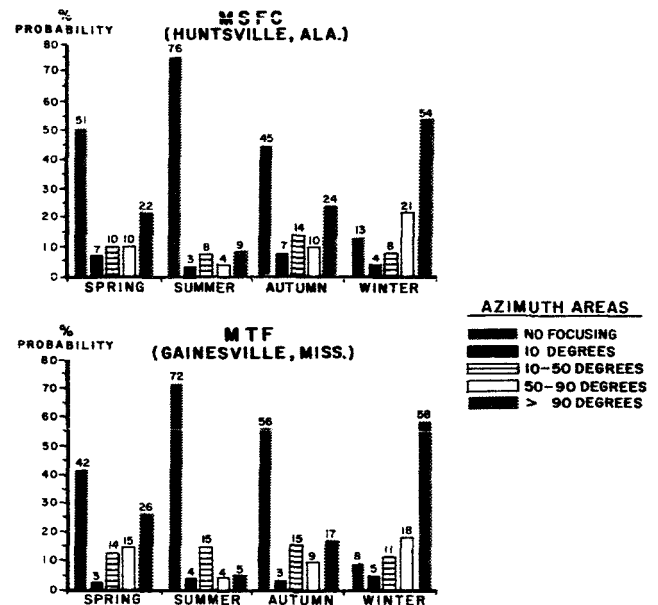


FIGURE 17. PROBABILITY OF AZIMUTH COVERAGE OF SOUND FOCUSING, MSFC AND MTF

affected by strong noise amplification. Figure 18 shows the distribution of focusing probabilities as a function of the azimuth around the whole wind rose for the four seasons at MTF. Again, the severity of focusing during winter is obvious, and the direction toward east is affected most. In contrast, the focusing during summer is spread almost evenly over the whole wind rose, with a low probability of less than 6 percent. Figure 19 shows the same presentation of azimuthal focusing distribution for MSFC. The overall features of areal focusing coverage are very similar to those at MTF. Figure 20 presents a comparison of winter focusing distribution for MTF and MSFC. It can be seen that the focusing around east is somewhat more severe at MSFC than at MTF.

E. MEASUREMENTS OF NONSTATIONARY SOUND PROPAGATION

The matching of a specific empirical sound-velocity profile with its simultaneously measured sound-intensity distance function proved to be greatly disappointing. A fair match of calculated sound-intensity amplification and relative sound-intensity maxima, measured in the field, could be obtained only in isolated cases. The reason for this failure of method was recognized early: the atmosphere as the medium of sound-wave propagation is not in a stationary condition, but is continuously changing [5]. The oversimplified mathematical model of the sound-ray-tracing method cannot do justice to these non-stationary conditions of the atmosphere, particularly because it uses only a two-dimensional concept. The

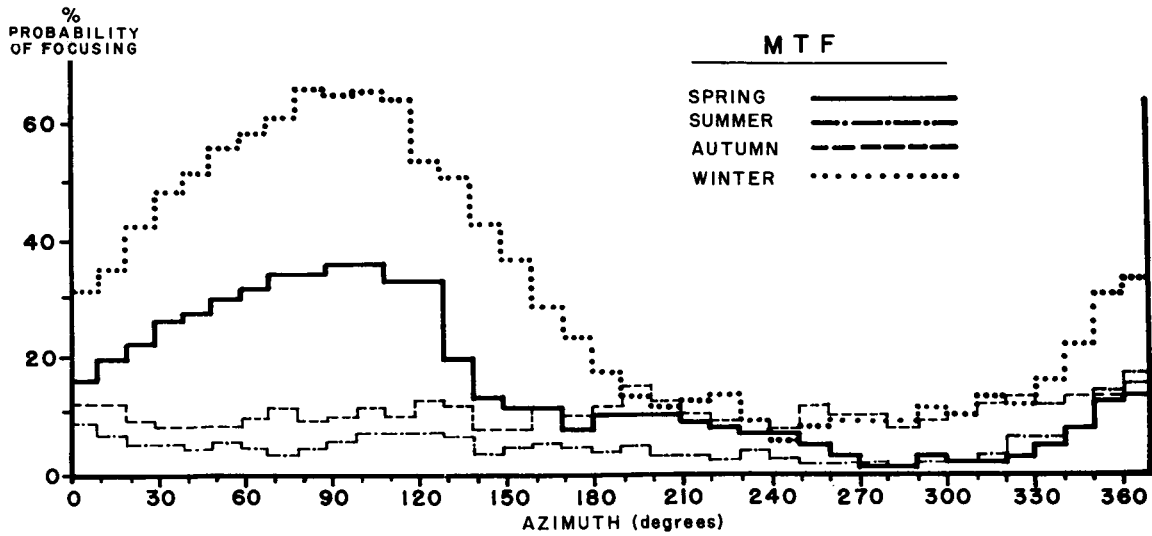


FIGURE 18. PROBABILITY OF SOUND FOCUSING, BY AZIMUTH; MTF

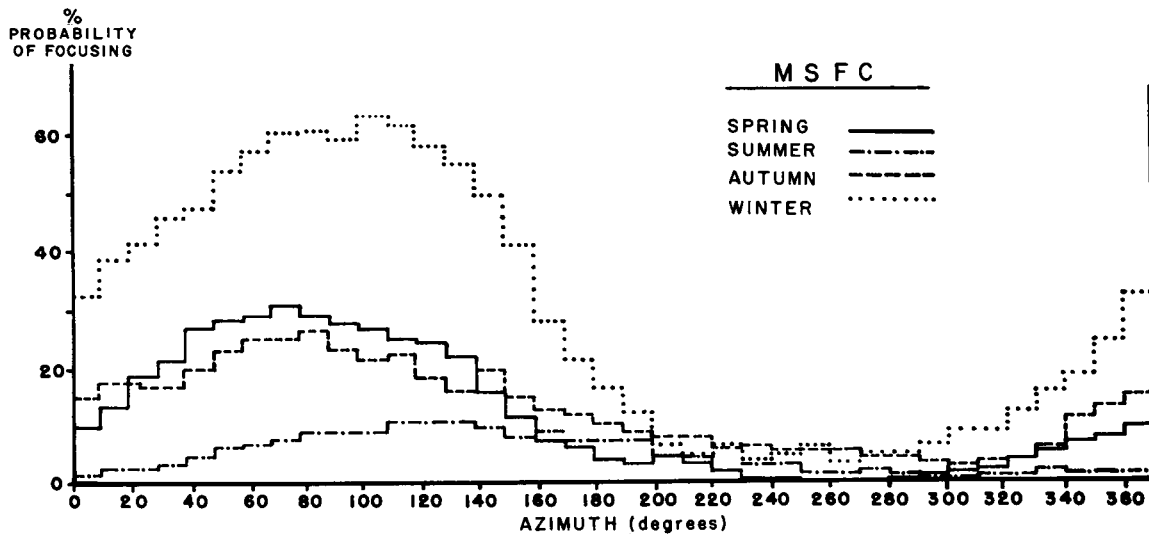


FIGURE 19. PROBABILITY OF SOUND FOCUSING, BY AZIMUTH; MSFC

extensive experience gained with the sound-intensity measurements at MTF strongly indicated the three-dimensional nature of the sound-propagation phenomena.

A novel approach for analyzing the nonstationary sound-propagation phenomena was conceived. The basic idea of this new method consists of the superposition of empirically determined "dynamic" perturbation functions on the pertinent characteristic sound-velocity profile types. Logically, these perturbation functions have to account for the nonstationary components of the individual sound-propagation conditions.

For the experimental task of establishing the "dynamic" perturbation functions, two measuring areas, each of about 600 by 600 meters side length, have been selected at MTF. One measuring area is situated on the 45-degree azimuth at a distance of 3.6 kilometers from the sounding horn, and the other measuring field is located on the 110-degree azimuth at a distance of 14 kilometers. In each of the two areas, a measuring network of five microphones has been laid out to cover the area in a cross-shaped pattern (Figs. 21 and 22). Background noise was reduced sufficiently by means of filtering networks and microphone screening (Fig. 23). The measuring series of the sound-propagation fluctuations were

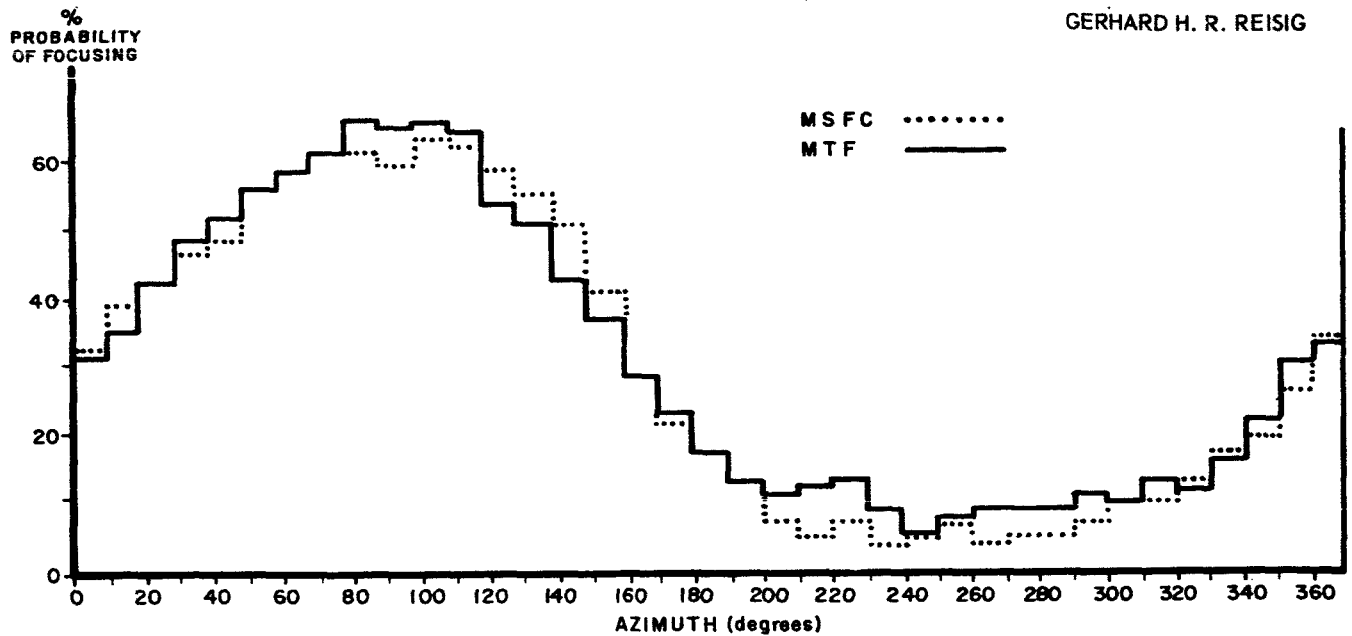


FIGURE 20. COMPARISON OF WINTER SOUND-FOCUSING PROBABILITIES, BY AZIMUTH; MTF AND MSFC

started in summer, 1965. The initial mode of operation of the whole measuring system is scheduled as a 10-second-sounding horn blast, with a 10-minute-repetition rate for 2 hours. Instrumentation design and data analysis of the multicross-correlation problem of the microphone array, supplemented by micrometeorological measurements in the microphone area, are handled by Tulane University Engineering School.

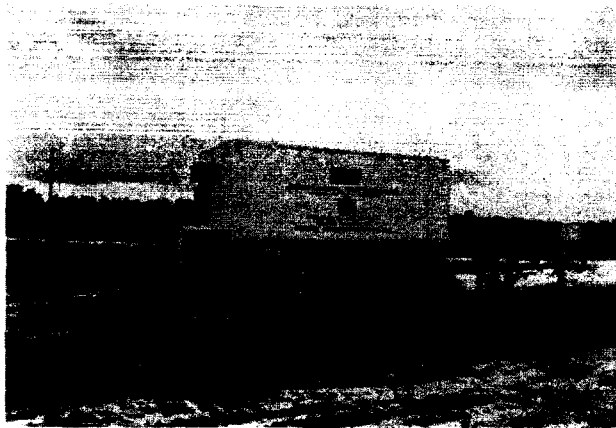


FIGURE 21. A SOUND-FLUCTUATION MEASURING STATION, MTF

A first sample of the sound fluctuation measurements in the microphone area at 3.6-kilometer distance from the sound source is presented in Figure



FIGURE 22. MICROPHONE CATWALK FOR SOUND-FLUCTUATION MEASURING FIELD, MTF

24. In Graph (I) it can be seen that the instantaneous sound-pressure levels at microphone stations 2 (center of field) and 4 (300-meter distance) differ as much as 19 decibels. Graph (II) represents the instantaneous SPL values at the five microphone stations, of the same area 10 minutes after the formation of the SPL pattern of Graph (I). Graph (III) demonstrates the SPL differences between Graphs (I) and (II). It can be recognized that the SPL values at microphone station 4 changed by 20 decibels within a period of 10 minutes. Therefore, the spatial SPL fluctuations over a 300-meter distance, and the temporal fluctuations over a 10-minute period, can attain the same magnitude of ± 20 decibels.

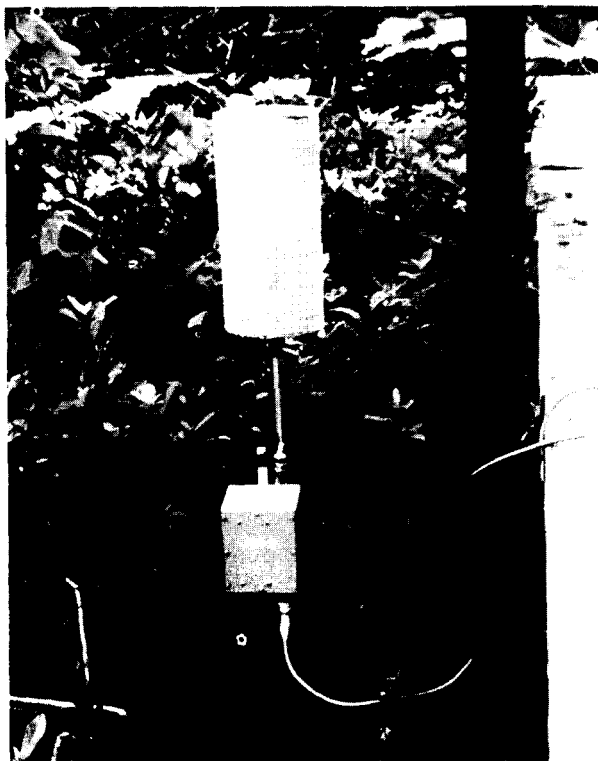


FIGURE 23. MICROPHONE SCREENING FOR SOUND-FLUCTUATION MEASURING FIELD, MTF

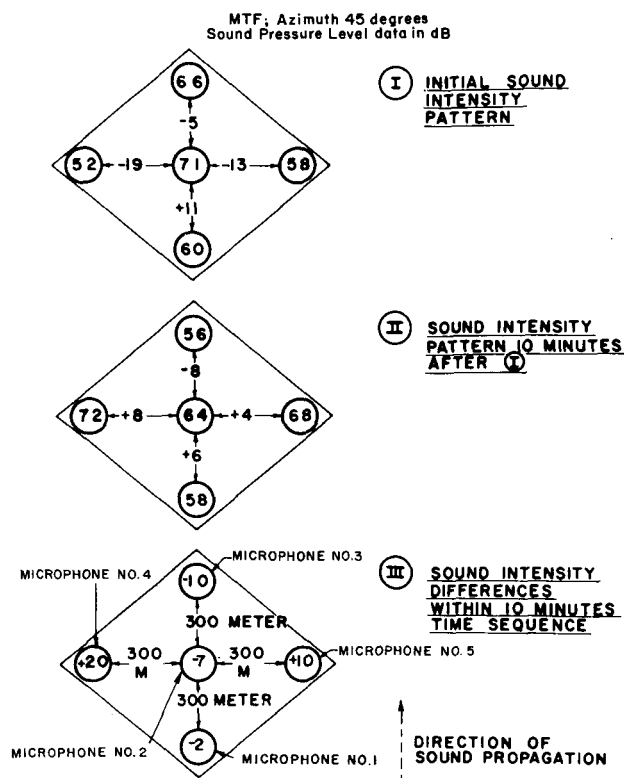


FIGURE 24. SOUND INTENSITY SPATIAL INHOMOGENEITIES AND TEMPORAL FLUCTUATIONS, MTF

IV. CONCLUSIONS

The extensive acoustic measuring program at MTF has generated, and still is generating for statistical completeness and reliability, a unique fund of acoustic far-field information. The novel

approaches in measuring techniques and data analysis, which are being applied in this project, give promise of providing comprehensive and reliable contingency tables for the relationships between atmospheric parameters and far-field sound intensities. These tables are a basic prerequisite for high-confidence sound-propagation forecasting for static rocket-firing tests.

REFERENCES

1. Pridmore-Brown, D.; and Ingard, U.: Sound Propagation into the Shadow Zone in a Temperature-Stratified Atmosphere Above a Plane Boundary. NACA TN 3494, 1955.
2. Pridmore-Brown, D.; and Ingard, U.: Tentative Method for Calculation of the Sound Field About a Source Over Ground Considering Diffraction and Scattering into Shadow Zones. NACA TN 3779, 1956.
3. Essenwanger, O.: On a System of Profile Types of Sound Speed in the Lower Atmosphere. Army Missile Command, Redstone Arsenal, 1965 (to be published).
4. Essenwanger, O.: On the Frequency of Returning Acoustic Rays and Focusing for Huntsville and Mississippi Test Facility. U. S. Army Missile Command Report No. RR-TR-66-2, Redstone Arsenal, Ala., 1966.
5. Sieg, H.: Ueber die Schallausbreitung im Freien und ihre Abhaengigkeit von den Wetterbedingungen. Elektrische Nachrichten-Technik 17(1940) 193 (No. 9).

TMX - 53486

N66 34348
ALBERT E. SCHULER

RESEARCH AND DEVELOPMENT IN INSTRUMENTATION FOR STATIC TESTING

By

Albert E. Schuler

SUMMARY

The varied MSFC research and development programs in instrumentation for static testing are summarized in this report. The work, done in-house and through contracts, is described under the categories of cryogenic fuel density measurements, mass flowmeters, liquid-level sensors, temperature-measuring instrumentation, damped accelerometers, digital transducers, and calibration systems.

Work on density measurements of cryogenic fuels, needed for better measuring accuracy, has resulted in the development of a very accurate point density sensor that uses a solid-state detector and a beta radiation source. Solutions to the special problem of measuring LH₂ density in suction lines are being evaluated. One densitometer under development uses x rays as a higher energy radiation source, which results in a faster response time.

MSFC initiated studies on mass flowmeters to meet the need for measurement of mass, rather than volume, of missile fuels. Several flowmeters, each with a different operating principle, are in various stages of development and test.

Investigations on liquid-level instrumentation is concerned with providing accurate and reliable discrete sensors for flow-rate determination. Two electronic level switches, one capacitive and the other conductive, have been developed successfully by MSFC. The most accurate and reliable all-purpose commercial unit tested by MSFC is an optical sensor.

Although the temperature of cryogenic fuels can be measured accurately, there is a problem of slow response because of test conditions. Sensor probes with fast response speed, based upon an MSFC design, have been developed and are being tested. In other in-house research on calorimeters, thermopiles were used successfully for radiation heat flux measurements.

An accelerometer operating by hydraulic damping, deformation of a composite mass, and signal generation by piezoelectric material, has been developed for use over higher frequency ranges without

ringing. For testing and calibrating high-frequency-range accelerometers, a new calibration system was developed; this uses either a constant-displacement or a constant-acceleration mode of operation. MSFC also has developed a portable accelerometer calibrator.

A digital pressure transducer has been developed; it has an 11-bit binary output, a resolution of 1 count in 2047, and an accuracy better than 0.1 percent. A 36-channel data recording system is being developed, using 20 of the new pressure transducers, 16 different electrical signals, a multiplexer, and very accurate DC amplifiers.

The calibration of ultrahigh-vacuum gages can be done now through a multistage pressure reduction method, devised through an MSFC-sponsored contract. Other investigations on measurement of extreme values deal with very low water-vapor content of pressurizing gases (less than 1 part per million) and calibration of load cells for 5-million-pound (22-MN) forces.

Significant work has been done in automatic calibration systems. One system, for calibrating pressure gages, uses a pressure balance and has a calibration accuracy of 0.05 percent. Another automatic system, a thermocouple calibrator, can automatically measure and print the output of 12 thermocouples.

I. INTRODUCTION

The research and development activities of the Instrument Development Branch of Test Laboratory, Marshall Space Flight Center, consist of in-house and out-of-house basic and applied research. This review is a summary of major research activities and achievements, and covers density measurements of cryogenic fluids, mass flowmeters, liquid-level gages, special temperature-measuring instrumentation, damped accelerometers, digital transducers, calibration of vacuum gages down to 10⁻¹⁰ torr (1.33 x 10⁻⁸N/m²), calibration of 5-million-pound (22.24-MN) load cells, and automatic calibration systems.

II. DENSITY MEASUREMENTS OF CRYOGENIC FUELS

During the first 25 years of work with liquid-propellant rockets, liquid oxygen (LOX) was measured quantitatively by weighing or by determining its volume with level gages. Volumetric and gravimetric values were converted through the use of density data in handbooks or international critical tables. The 0.5-percent disparity between calculation and measurement was attributed to measurement inaccuracy. In 1958, a test with repeated weighing at overflow demonstrated that LOX density changed with the time. A more elaborate measuring program established that the density of LOX in a missile tank differs from the density given in the handbooks. At the conditions for which the handbooks stated a density of 1.14 g/cm^3 , accurate measurements of LOX showed 1.333 g/cm^3 , a difference of 0.6 percent. There was an evident need for instruments to measure LOX density. Consequently, a research contract was awarded to Franklin Systems, Inc., with the result that prototype density measuring instruments were developed. These measured the average density of LOX in tanks of various diameters, using cobalt 60 as a radiation source at one side of the tank and a scintillation counter at the opposite side (Fig. 1). When tank diameters were too big, measurements were made across a secant instead of the diameter (part A, Fig. 1).

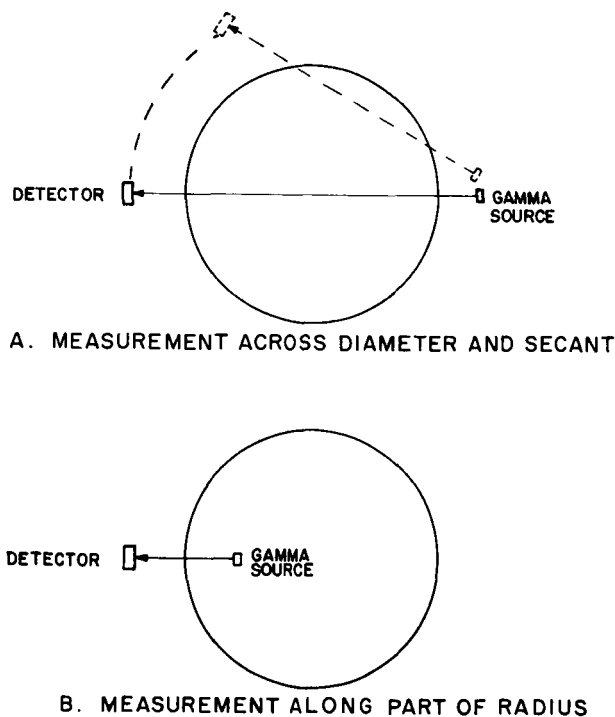


FIGURE 1. DENSITY MEASUREMENT OF CRYOGENIC FUEL IN A TANK

The scintillation counters, particularly the photomultiplier portion, were insufficiently stable. Therefore, a servo-type self-adjustment, with an alpha radiation source on the detector side, was added as a reference. Better repeatability could be obtained with this compensating feature, but for field use the equipment still was not reliable enough.

The contract was extended to learn whether other detectors would be better than scintillation counters, and the contract study showed that a xenon-filled ionization chamber was better. Under constant temperature, the repeatability of a densitometer with an ion chamber is 0.1 percent. The idea of compensating a scintillation counter with an alpha source, as mentioned, is now being used by several companies for other nuclear instrumentation.

An isotope radiation source submerged in LOX is represented by part B of Figure 1. With this arrangement it was possible to determine the average density of different layers of LOX next to the tank wall, in order to get information about the density profile across the tank. However, all the arrangements with average density measurements along a diameter, secant, or part of a radius were insufficient for determining density stratification. Therefore, a new research and development program to develop point-density sensors was started. These sensors use beta radiation from a strontium 90 radiation source, and a solid-state detector close to the source (Fig. 2). The entire unit is submerged in LOX at different locations in the tank so that the LOX density profile can be determined. The individual units are reliable for LOX measurements; a system using six detectors has been delivered to MSFC and is now being tested. The same method was used for point-density measurement in liquid hydrogen (LH_2), but more research had to be done, mainly in reference to resistance contacts and epoxy resins, so that the sensor could be made to withstand the low temperature. These problems have been solved, and LH_2 point-density measuring units in a 10-channel system will be available soon. For LOX and LH_2 , the accuracy of these point-density sensors is about 0.1 percent for 10-second counting time, and about 0.2 percent for 1-second counting time.

When LH_2 was selected as the propellant for upper stages of Saturn vehicles, the deviations of LH_2 densities from handbook data were expected to be worse because the density of LH_2 changes 1.6 percent per degree Kelvin. However, it was found that the handbook density data for LH_2 agreed much better with the densities as measured for LOX. The explanation is that LH_2 is in vacuum-jacketed tanks, similar to the thermos flasks used in the laboratories where density data for handbooks are determined,

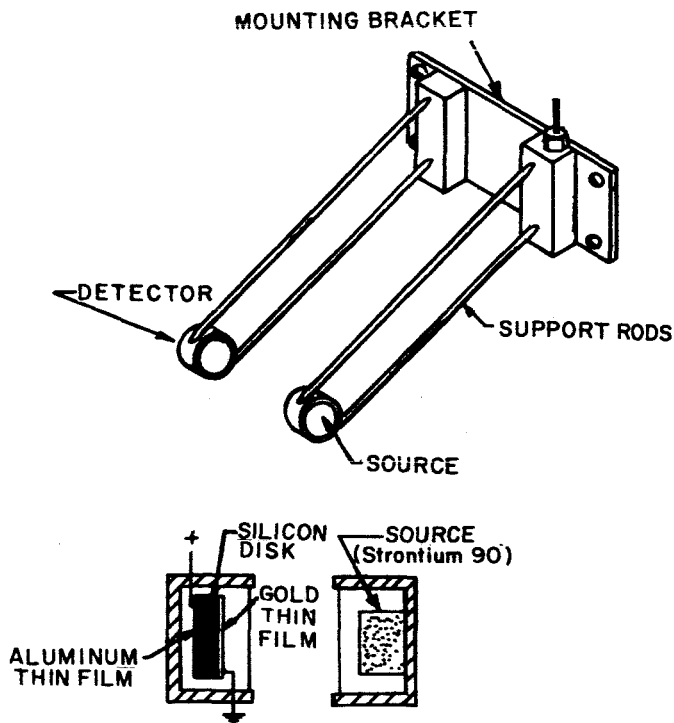


FIGURE 2. DENSITY MEASUREMENT OF CRYOGENIC FUEL AT A POINT WITHIN THE TANK

while LOX in missiles is in uninsulated tanks and, therefore, because of the heat influx, the density deviates up to 0.6 percent.

These observations are true for tank containment. In regard to LH_2 suction lines there are other significant problems caused by two-phase conditions and density instabilities. Accurate measurements require densitometers with higher speeds of response than are needed for tanks. There is a current contract to develop a densitometer for LH_2 in the S-IVB suction line. In this development, x rays are used instead of isotopes to provide more radiation energy. Greater energy results in faster response. In addition, the radiation hazards are reduced, since x rays can be cut off. Figure 3 shows the arrangement schematically. The two-beam arrangement compensates for changes in the x-ray unit. An aluminum or a beryllium disk can be used as a calibration absorber by inserting it into the beam path.

The unit has been constructed for regular use and is in its final test phase. Indications are that 0.1-percent accuracy and a 0.5-second time constant have been achieved. Pending completion of testing, MSFC is using a less accurate instrument for making some measurements in the S-IVB suction line. This instrument uses available components: cesium 137 as a radiation source and an ionization chamber as a detector. The instrument has an acceptable repeatability for comparisons, but it cannot be used for absolute density measurements.

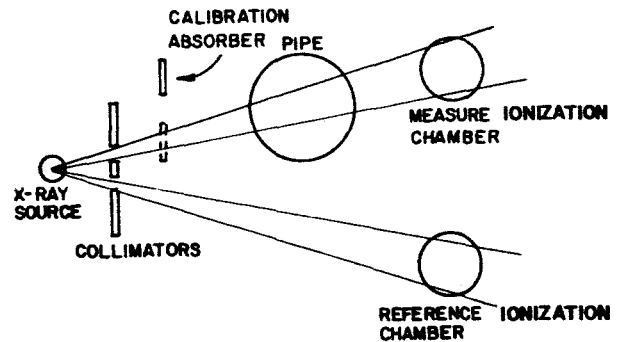


FIGURE 3. DENSITY MEASUREMENT OF LH_2 IN A PIPE, USING SPLIT X-RAY BEAM

III. FLOWMETERS

The turbine-type, volumetric flowmeter has been used for flow measurements during the last two decades. These meters have been improved steadily and are now very accurate and reliable. However, the energy content of missile fuels is a function of the mass rather than of the volume.

Because of the uncertainty of density data as a function of pressure and temperature, and the increase in errors when three parameters must be measured to determine one value, the search for direct mass flowmeters was intensified.

A contract for the study of mass flowmeters for all propellants was awarded to Armour Research Institute (now IIT) by the Army Ballistic Missile Agency in 1958. On the basis of information provided by the study (which summarized the state of the art of flowmeters), a 1-inch (2.54-cm) GE angular momentum flowmeter was purchased for investigation by Armour. In addition, a contract was awarded to Potter Aeronautic Corp. for the production of a prototype gravimetric quantity meter for filling control. The Potter meter uses a standard volumetric turbine flowmeter and a float-operated densitometer which starts and stops the counting of pulses from the turbine flowmeter once every minute for a duration determined by the density. When this meter had been developed into an accurate and reliable instrument, MSFC had to abandon its interest in it for two reasons: Jupiter work had been transferred to the US Air Force, and a decision had been made to use level switches and differential pressure measurements for Saturn fuel filling control because of the desirability

of obtaining volumetric and gravimetric data. However, the Potter meter has now been found useful for filling control of Apollo storable propellants.

A more elaborate study, development, and evaluation contract for LH₂ mass flowmeters was initiated in 1961 with Wyle Laboratories. As required by the contract, a well designed calibration facility was created. Illustrated diagrammatically in Figure 4

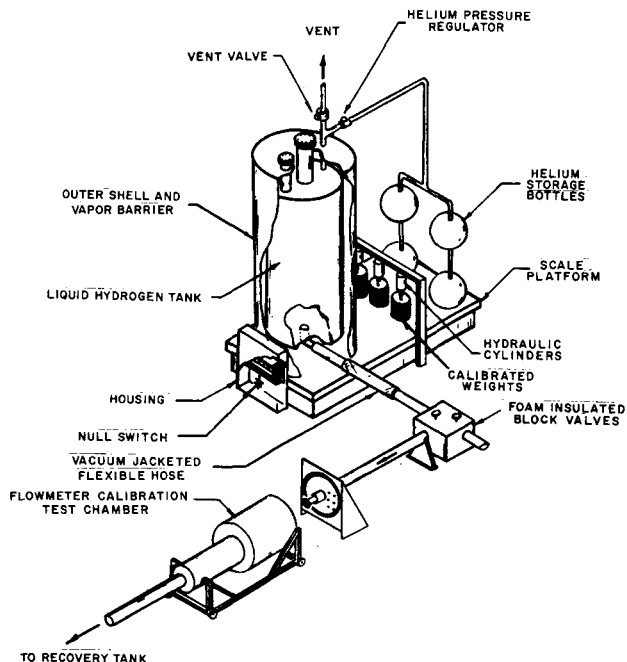


FIGURE 4. LH₂ FLOWMETER CALIBRATION STAND

is an LH₂ tank (with the usual valves for filling, drainage, pressurization, and venting) resting on a mechanical weighing scale. The tank is within a larger container and is insulated from it with glass wool (5 cm thick) and plastic foam (15 cm thick). Additional plastic foam insulation at the top and bottom covers the valves, fuel lines, etc. To eliminate the need for correction of the weight of pressurization gas (helium), there are four spherical helium storage tanks on the scale. Calibration masses in the form of drop weights are suspended on a gallows across the scale platform. The scale is used as a null detector rather than as an absolute-weight-measuring device. The tare is so adjusted that a capacitive null switch operates after constant flow is achieved. The null switch starts timers and counters or other flowmeter output recording systems after the calibration is started. Then the drop weights are lowered to the platform of the scale, and when a

mass of LH₂ equal to the mass of the drop weights has been taken from the tank for flowmeter calibration, the null switch operates again and stops the timers and counters. In this way the LH₂ mass is directly compared with the mass of the drop weights. The vacuum-jacketed flexible hose provides fairly free movement of the scale, and the null switch always operates at the same platform position, which results in an accuracy of 0.1 percent. The flowmeters are inserted in a vacuum-jacketed calibration chamber big enough to accommodate any type flowmeter of the 3-in. (7.6-cm) class, which is the size of flowmeters investigated in this program. Two-phase flow is obtained by adding helium gas, and the mass measurement of the two-phase flow also is 0.1 percent accurate.

During this development program, the following five mass flowmeters were tested, evaluated, and modified.

a. A gyroscopic mass flowmeter (Decker Corp., Fig. 5) passes the liquid through a circular loop, thus simulating the rotating flywheel of a gyroscope. A motor-driven eccentric cam forces the loop to precess in an oscillating manner; the resulting rectangular torque causes a displacement of the loop, which is restrained by torsion members. The displacement of the loop is measured as a function of mass flow.

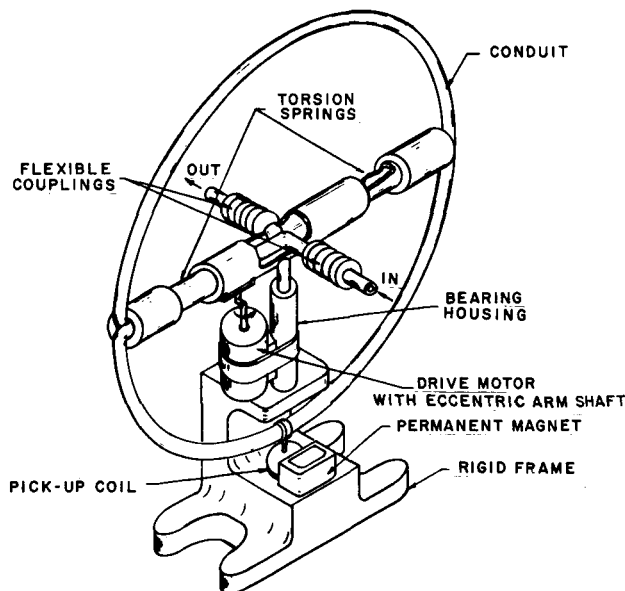


FIGURE 5. GYROSCOPIC MASS FLOWMETER (DECKER)

b. A twin-turbine mass flowmeter (Potter Aeronautics, Fig. 6) uses two turbines with different

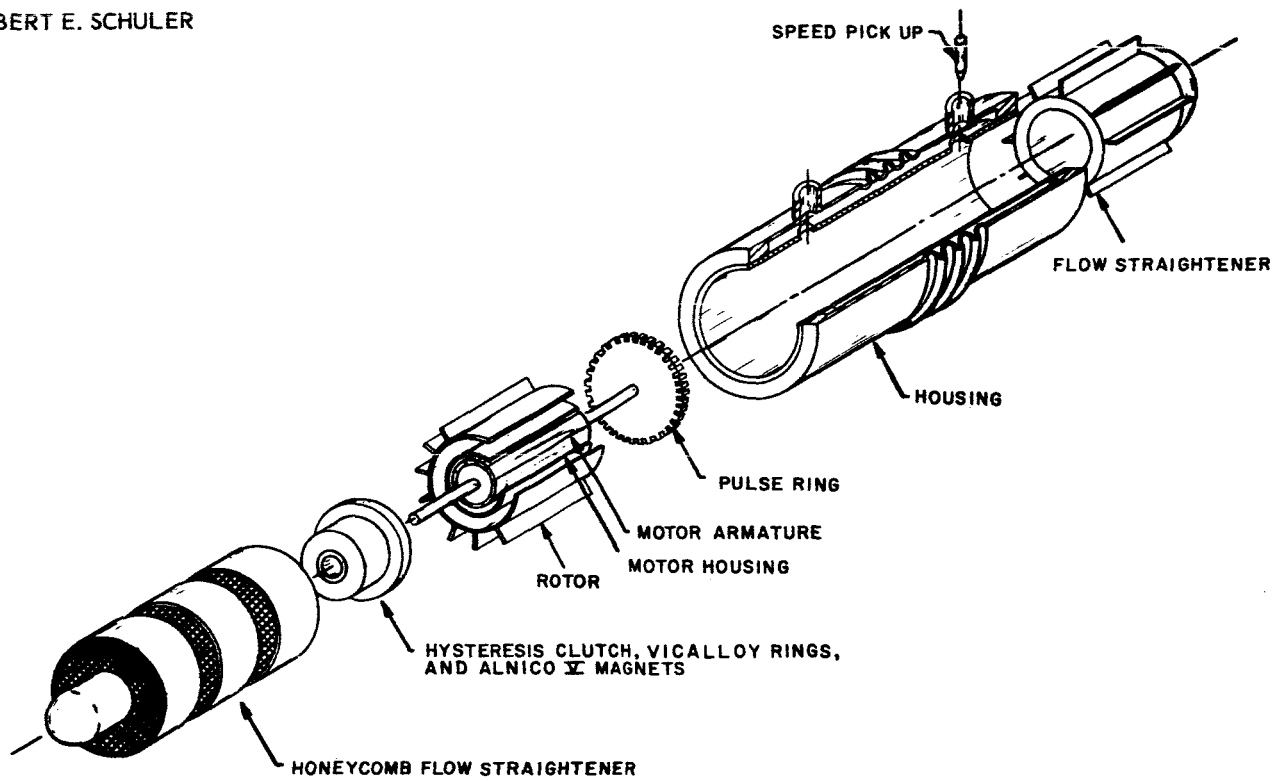


FIGURE 8. CONSTANT-TORQUE MASS FLOWMETER (WAUGH)

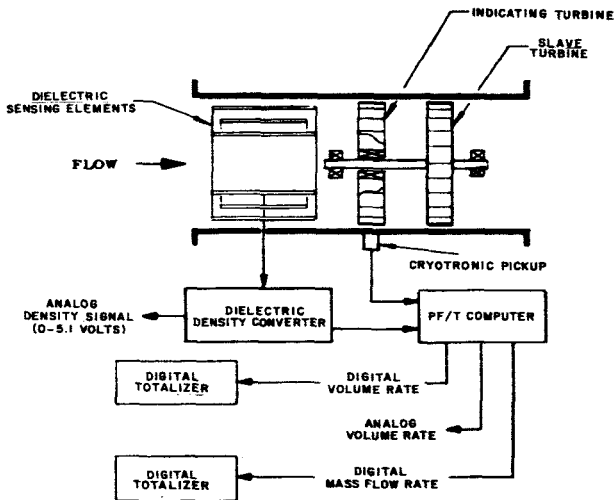


FIGURE 9. INFERENTIAL MASS FLOWMETER (QUANTUM DYNAMICS)

conditions the flow pattern so that detrimental line effects are reduced or eliminated. In the Quantum meter it serves as a slave turbine, rotating the shaft of the measuring turbine. The purpose of this arrangement is to reduce bearing drag. The Quantum densitometer system is good in principle, but it often

fails to withstand the rough working conditions. When this deficiency is corrected by the manufacturer, the meter may be one of the best of the mass flowmeters.

The ideal flowmeter would have no moving parts and no obstructions in the line. Under contract with MSFC, Bendix Corp. is developing a capacitive flowmeter without moving parts (Fig. 10). The meter uses a wire mesh as a sensor for the ρv^2 term of the flowing liquid. The tendency of the mesh to move under the force of liquid flow changes a capacitance, causing electromagnets to initiate a servo-directed compensation. Honeycomb grids measure the liquid density through the capacity change, and a computer mixes these measurements to yield mass flow data. This capacitive meter is in the prototype stage, and is being tested and improved.

Neptune Meter Co. has developed a flowmeter which operates on a boundary-layer heat-conductivity principle and has no obstruction in the line. (This work has not been done under contract.) Metering based upon a heat-conductivity principle may be expected to have a relatively slow response. However, MSFC has purchased one of the Neptune meters and it will be tested by the Wyle calibration facility for speed of response and accuracy.

blade angles that are coupled with a torsion spring and so rotates as a unit. The phase angle between the two turbines, or the time period between passing of fixed reference points on the two turbines, is measured as function of the mass flow. The velocity of the coupled turbine assembly is proportional to the volumetric flow.



FIGURE 6. TWIN-TURBINE MASS FLOWMETER (POTTER)

c. The angular momentum mass flowmeter (General Electric Corp., Fig. 7) uses an impeller, driven at constant speed by a synchronous motor, to impart an angular velocity to the passing fluid. A turbine, immediately downstream, absorbs the angular momentum of the fluid, and its deflection against a spring is measured as a function of the mass flow.

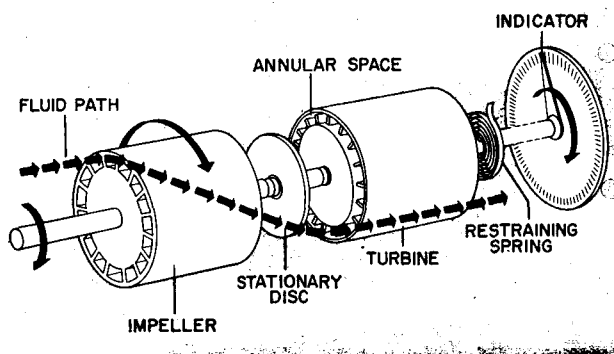


FIGURE 7. ANGULAR MOMENTUM MASS FLOWMETER (GE)

d. A constant-torque mass flowmeter (Waugh Engineering Co., Fig. 8) uses a turbine with zero blade angle, driven at constant torque by a synchronous motor with a magnetic hysteresis clutch. The speed of the turbine decreases inversely with increasing flow rate.

e. An inferential mass flowmeter (Quantum Dynamics, Fig. 9) measures flow volumetrically. It has a slave turbine to rotate the shaft for the sensing turbine to reduce inaccuracies from bearing drag, and it utilizes a high-frequency wave-absorption principle to detect the rotation of the turbine without magnetic loading. Fluid density is measured with a capacitive sensor, and the two signals for volumetric flow and density are combined into a signal for mass flow in a computer which also has outputs for analog density, analog velocity, digital mass flow, and digital volume flow.

The single-phase repeatability of the five flowmeters is shown in Table I. A repeatability of 0.1 percent was desired, but 0.5 percent was the best obtained. Although short of the desired accuracy, this achievement is useful in indicating the direction the work must take for attaining the 0.1-percent accuracy.

TABLE I. REPEATABILITY OF MASS FLOWMETERS DURING CALIBRATION WITH LIQUID HYDROGEN

Flowmeter	Repeatability (%)
Decker Corporation Vibrating gyroscopic mass flowmeter	± 0.9
General Electric Company Angular momentum mass flowmeter (Using bypass principle)	± 0.5 ± 1.0
Potter Aeronautical Corporation Twin-turbine mass flowmeter	± 0.5 $\pm 0.12^*$
Waugh Engineering Company Constant-torque mass flowmeter	± 0.5
Quantum Dynamics Corporation Inferential mass flowmeter	± 0.5 $\pm 0.1^*$

* Volumetric data

For volumetric measurement (Quantum and Potter meters), a repeatability of 0.1 percent was shown, which is the best accuracy obtainable as yet for LH_2 measurement. This accuracy and the versatility of the meters in being usable for gravimetric and volumetric measuring are distinct advantages. The additional turbine in both meters probably

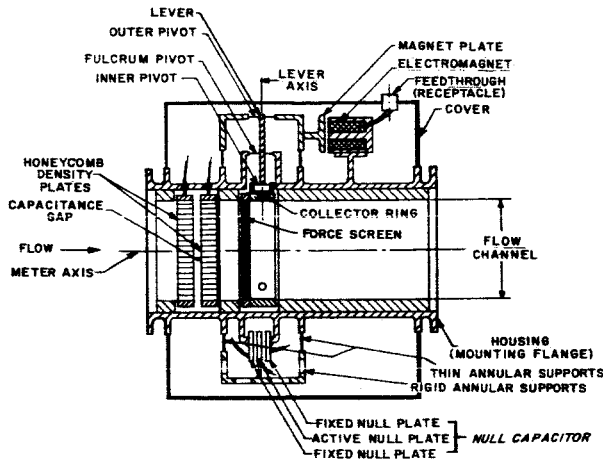


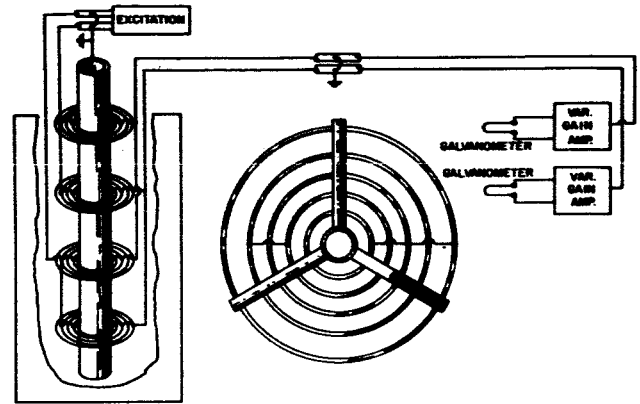
FIGURE 10. CAPACITIVE MASS FLOWMETER (BENDIX)

A considerable amount of research on the applicability of nuclear methods to mass flowmeter design has been done by government agencies and private industry. It was not evident until recently, however, that nuclear methods were suitable for MSFC applications. As a result of new advancements in nuclear technology, the idea of flowmeters based upon nuclear principles has appeared to warrant study by MSFC; therefore, it has initiated a feasibility study through a contract with Industrial Nucleonics Corp.

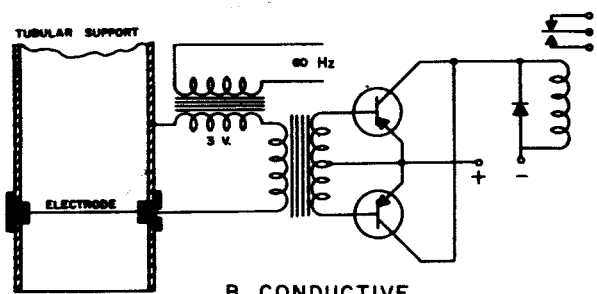
IV. LIQUID-LEVEL INSTRUMENTS

Most of MSFC research and development in the field of liquid-level measurements was done in-house, with some research funds being used to buy commercial products. The accuracy and reliability of continuous liquid-level gages were well advanced even during the early days of rocket development. It was obvious, however, that discrete liquid-level sensors would have to be used for flow rate determinations because the difference between two levels is required for flow rate, and less than 1-percent accuracy was obtainable with continuous-level gages. The special advantage of level switches is in their absolute accuracy, and the percentage accuracy of liquid-level measurements with discrete level sensors increases proportionally with the height of the tank. Better than 0.1-percent accuracy in flowmeter calibration can be obtained at calibration stands with tall tanks. At test stands flow rate determination is less accurate because of the turbulent surface of the liquid fuels.

Originally, float-operated level switches were used for LOX and alcohol measurements. By 1955, very accurate and reliable all-electronic level switches had been developed. Two types, capacitive and conductive, are illustrated diagrammatically in Figure 11.



A. CAPACITIVE



B. CONDUCTIVE

FIGURE 11. CAPACITIVE AND CONDUCTIVE DISCRETE LIQUID-LEVEL SENSORS

The capacitive switch (A, Fig. 11) uses rings as electrodes of a capacitor. Alternate rings are interconnected to serve as the two electrodes of a capacitor that varies its capacitance, depending upon whether there is liquid or gas between the rings.

The conductive switch (B, Fig. 11) uses a wire across a pipe. The wire is insulated from the pipe, and the resistance between wire and pipe decreases when the wire is submerged in conductive liquid. Water, or even missile fuel with much lower conductivity, operates the sensors.

Since private industry as well as aerospace agencies had been conducting research and development to produce better discrete liquid-level sensors, MSFC decided to replace its "homemade" probes with

commercial ones. Therefore, it bought ten each of five different types and tested them. A summary of the accuracy tests is given in Table II.

TABLE II. REPEATABILITY OF COMMERCIAL DISCRETE LIQUID-LEVEL SENSORS IN DIFFERENT LIQUIDS

Sensor Operating Principle	Repeatability millimeter (inch)			
	Water	RP-1 Fuel	LN ₂	LH ₂
Capacitive		±0.127 (±0.005)	±0.152 (±0.006)	±0.152 (±0.006)
Optical	±0.102 (±0.004)	±0.102 (±0.004)	±0.305 (±0.012)	±0.762 (±0.030)
Magnetostrictive	±0.305 (±0.012)	±0.305 (±0.012)	±0.254 (±0.010)	±0.305 (±0.012)
Piezoelectric	±0.330 (±0.013)	±0.102 (±0.004)	±0.102 (±0.004)	±0.254 (±0.010)
Thermal				±0.356 (±0.014)

Most of the switches were very accurate and reliable when tested in the laboratory, but they were much less so when used at the test stands. Therefore, the accuracy data shown in Table II do not reflect reliability in the field. The optical sensor (Fig. 12) appeared to be the most accurate and reliable sensor for all-purpose use. Many were used at various test facilities, but the "homemade" switches still seem to be the most reliable.

The results of work by MSFC and Trans-Sonics, Inc., have been combined to produce a continuous liquid-level gage, now used in the S-ICT missile at the MSFC test stand. Trans-Sonics research was in servo bridge-balancing; MSFC contributed its experience in dividing the level gage and using the sections in different parts of the bridge.

V. TEMPERATURE-MEASURING INSTRUMENTATION

In the past, MSFC did a considerable amount of research on temperature sensors as part of its thermal instrumentation program. Not much significant advance was made for thermocouples with various materials, or for oscillating crystal sensors. More success was achieved with platinum resistance thermometers, which were greatly improved through the work of private industry, done partly in close cooperation with MSFC.

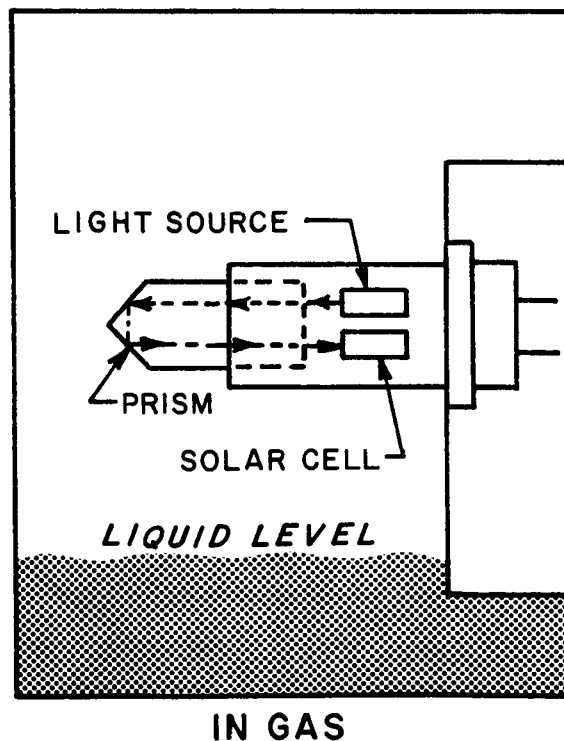
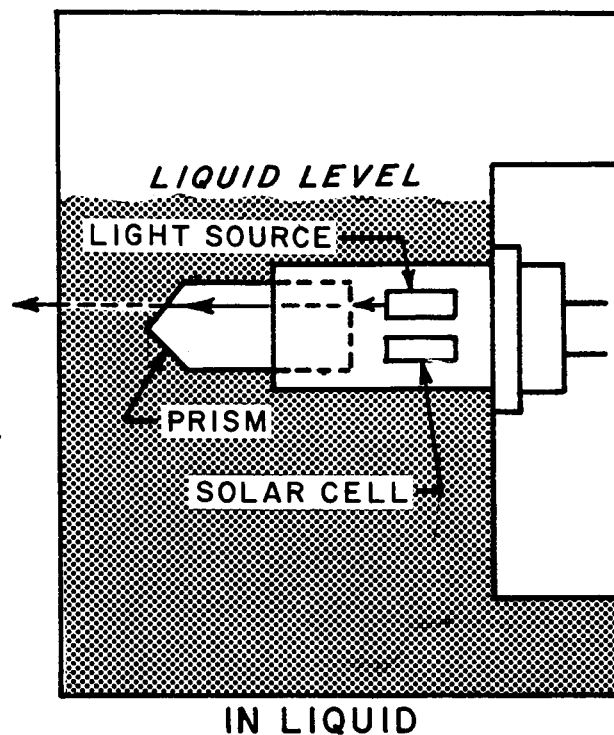


FIGURE 12. OPTICAL DISCRETE LIQUID-LEVEL SENSOR

At present, very accurate and reliable temperature measurements of cryogenic fuels can be made. However, the speed of response still is a problem. The temperature sensors are slow because the time constant is increased by the sturdy sensor-holding devices, which are necessary because of test-stand vibration. The following conditions illustrate the problem. The temperature of LOX in a Saturn I tank was -297.4°F (90.15°K), while the temperature of gaseous oxygen was approximately 400°F (478°K). When the LOX level dropped below the sensor, the sensor did not quickly indicate the high temperature of the gaseous oxygen but instead often indicated a lower temperature than the LOX, -300°F (89°K), because of LOX evaporation. The speed of response was improved with an MSFC-laboratory-devised thermocouple (Fig. 13). This has a 30-gage copper-constantan wire suspended in a slingshot-like bracket of minimum practical thickness. Its time constants are 0.6 second when submerged in LOX, 1.3 second when emerging with the bracket above the wire, and 2.6 seconds when emerging with the bracket below the wire.

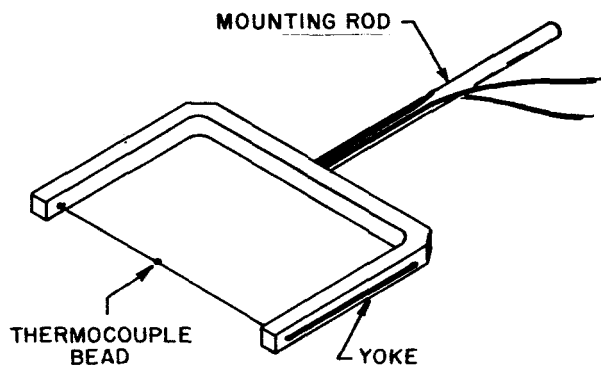


FIGURE 13. SLINGSHOT THERMOCOUPLE

In an attempt to obtain a better thermocouple than this slingshot type, MSFC had two companies make special resistance thermometers for faster speed of response. The sensors that were made had very thin wires and fragile holding arrangements. Since they were more fragile than the slingshot thermocouples and there was no improvement in the time constant, a research contract was awarded to another company for the development of sensors with the following specifications: a sensitivity of 0.01°F (0.0056°K); an accuracy of 0.05°F (0.0278°K) in the range of -425° to -410°F (19.3° to 27.6°K); and an accuracy of 0.5 percent at -425°F (19.3°K), with a response speed of 0.5 second. These sensors are being tested.

Considerable improvement in heat flux measurements was achieved by in-house research on calorimeters. The use of thermopiles for radiation heat flux measurements was one of the major achievements.

VI. DAMPED ACCELEROMETERS AND ACCELEROMETER CALIBRATION SYSTEMS

Accelerometers usable over higher frequency ranges without ringing were needed for more accurate vibration measurements. Gulton Industries studied this problem and developed a damped accelerometer (Fig. 14). The seismic mass of this instrument is

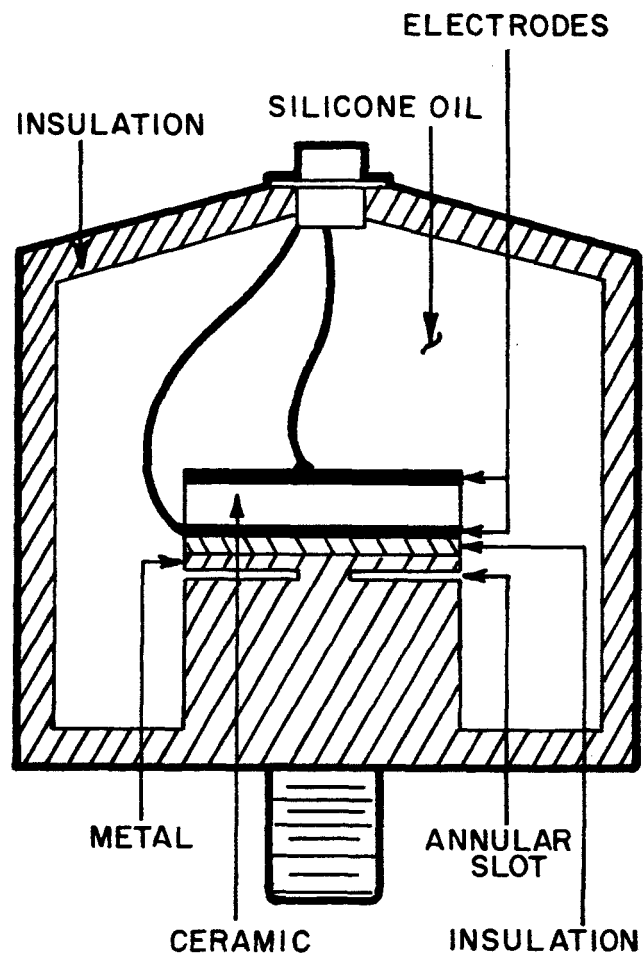


FIGURE 14. DAMPED ACCELEROMETER

a diaphragm-like structure composed of piezoelectric material and metal, supported at its center by a

column. Upward forces cause the composite mass to deform. As the edge of the material moves downward, the width of the annular slot decreases, forcing the silicone fluid to flow out. A downward force increases the width of the slot, and the fluid flows back into the slot. Thus, damping of the motion is achieved by the pumping of silicone in and out of the annular slot. Electric signals are generated by the bending of the piezoelectric element. The frequency response of these accelerometers is nearly flat up to 15 kHz (Fig. 15).

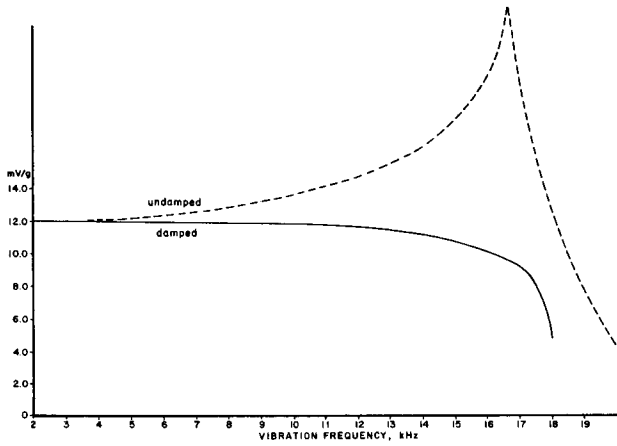


FIGURE 15. FREQUENCY CHARACTERISTICS OF DAMPED ACCELEROMETERS

A new calibration system was developed for absolute calibration and testing of accelerometers with high-frequency range. The calibration system, diagramed in Figure 16, uses either a constant-displacement or a constant-acceleration mode of operation. For constant displacement an interferometer measures fixed increments of displacement, and the shaker is regulated until a certain displacement is reached. When the output of the photomultiplier reaches null, the fringe disappearance indicates that the displacement of the shaker table is 4.11 microinches ($0.104 \mu\text{m}$) or a multiple of it. The 20-Hz oscillator modulates the intensity sensed by the photomultiplier, which results in higher sensitivity. The instrument accuracy is about 1 percent. The constant acceleration mode of operation uses the accelerometer in the table as a standard. This method is much less accurate, but it requires less time.

MSFC also uses a portable accelerometer calibrator, which it developed in-house (Fig. 17). The instrument uses a resonant frequency of a beam excited up to 20 gauss by an electromagnet and oscillating at a constant frequency of 120 Hz.

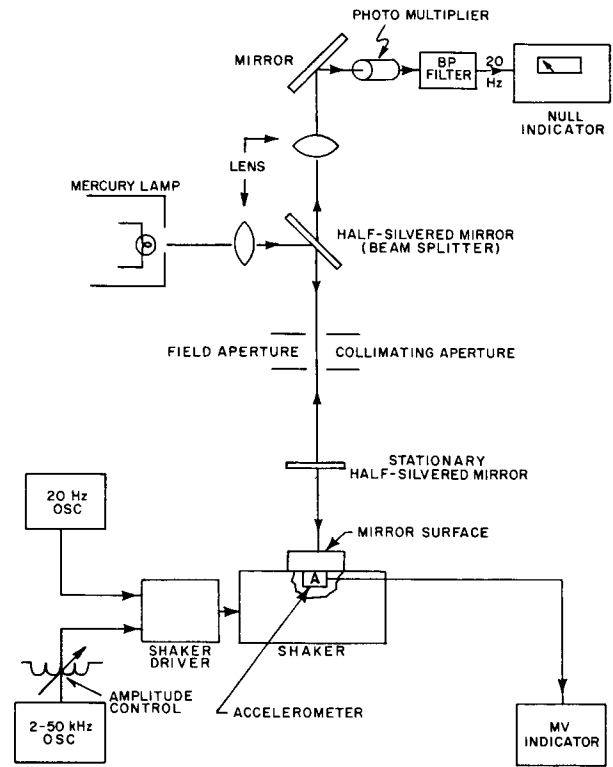


FIGURE 16. ACCELEROMETER CALIBRATION SYSTEM

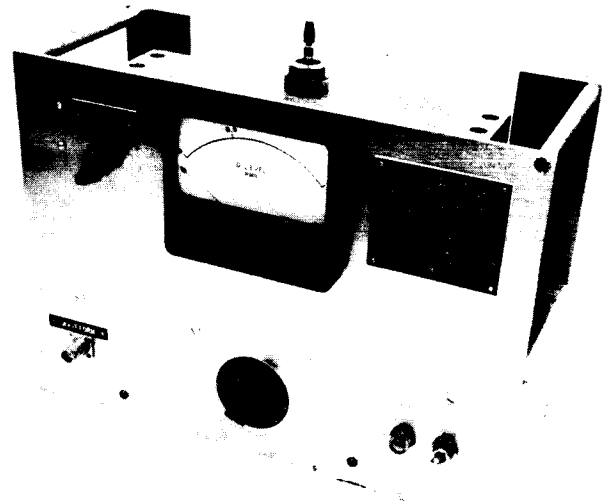


FIGURE 17. PORTABLE ACCELEROMETER CALIBRATOR

The application of laser techniques to accelerometer calibration is being studied by National Bureau of Standards, under contract.

VII. DIGITAL TRANSDUCERS

The "era" of digital transducers started in response to increasing accuracy requirements, the need for handling more channels with fewer cables, and many other reasons. In the field of digital measurement, MSFC and Giannini Controls Corp. developed a very accurate digital pressure transducer. In the measuring system, illustrated in Figure 18, the transducer uses a force balance and an up-down counter principle. The bellows convert the pressure into force, which is balanced by an electromagnetic torquer. A special two-bellows arrangement with slightly different effective areas of the bellows increases sensitivity and decreases the force; the result is a desirable reduction in the required torque. When there is an unbalance in the force from bellows and torquer, a differential transformer null detector gives signals to the counter, and a digital-to-analog converter conditions the signal of the counter to change the current for the electromagnetic torquer until it balances the force of the bellows. The counter also provides digital output in binary form (11 bits).

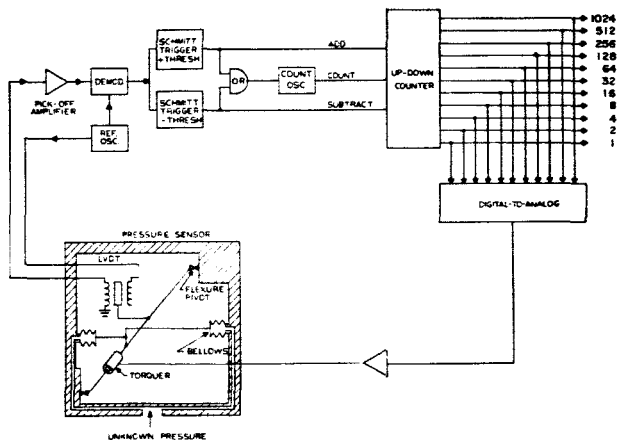


FIGURE 18. DIGITAL PRESSURE TRANSDUCER

The prototype digital pressure transducer which was delivered has a resolution of 1 count in 2047 and an accuracy of better than 0.1 percent. A great interest in this transducer was indicated by the inquiries from within the United States and from other countries.

Giannini Controls, under a development contract, is to provide a 36-channel digital transducer and data recording system. Four channels each will be used for pressures of 1, 10, 100, 500, and 1000 psi (0.69,

6.9, 69, 345, and 690 N/cm²), respectively, and four channels each will be used for resistance thermometers, strain gages, thermocouples, and DC voltages. Electrical null balance and the same up-down counter principle (as in the other pressure transducer) are used for the electrical measurements. A digital multiplexer and magnetic tape recorder are included in this system. Most of the system components have been completed, with some features being improved; therefore, this research and development may be termed an important achievement in the field of digital transducers.

The pressure transducer discussed has a binary-coded digital output. MSFC also initiated the development of a miniature analog-to-digital converter to be used next to the transducer. In this system, developed by Trans-Sonics, Inc., the output of the transducer is fed to a paractor, which provides parametric amplification and comparison for digital conversion of very small signals. The paractor is part of the analog-to-digital conversion system and has to be in the immediate vicinity of the transducer so that electrical noise effects can be avoided. The rest of the system called logic can be several hundred feet away. For some applications, the paractor, which takes up 8 cm³ (0.5 in.³), will be constructed like an electrical connector so that it can be attached as an integral part of the transducer.

Packaged with the logic is a multiplexer which has been developed to scan the digital output of 120 channels and to send these signals through two pairs of shielded cables to the blockhouse. This will eliminate the noise effect on low-level signals, and it will make it possible to handle many more channels with fewer cables.

Since the research for a small analog-to-digital converter resulted in the development of the very promising paractor, the contract was extended for the development of a DC amplifier. Two prototype DC amplifiers have been delivered, for which Trans-Sonics, Inc., claims an accuracy of 0.01 percent under constant conditions, a zero drift of about 0.01 percent for a 10° F (5.56° K) temperature change, and a slope change of about 0.01 percent for a 3° F (1.67° K) temperature change. Tests and probable modifications or improvements are pending.

Twenty-five years ago, transducers were developed with slide wire, capacitive, magnetostrictive, differential transformer, or variable-reluctance pickups. Fifteen years ago, the strain-gage pickup started a new measuring technology, in which increasing numbers of strain-gage pickups were used for various measurements. Five years ago, the

idea of digital transducers gained momentum, and it can be expected that five years from now the direct digital transducer systems will have replaced many of the present strain-gage pickups and analog-to-digital conversion systems.

VIII. ULTRAHIGH-VACUUM CALIBRATION SYSTEM

In the calibration of vacuum gages below 10^{-5} torr (1 mN/m^2) the usual comparison with a standard cannot be used because none exists for this very low pressure. A research contract with National Research Corp. was initiated by MSFC to establish principles and develop equipment for creating the low pressures of accurately known values needed in calibrations of vacuum gages. The calibration system that was devised (Fig. 19) uses a series of three individually pumped pressure chambers, with the pressures decreasing in a ratio of 100 to 1 from chamber to chamber. The pressure of each chamber is kept constant by continuous pumping, and the pump and chamber interconnections have pressure attenuating orifices of known conductance. Thus, the pressure attenuation of each stage is mainly determined by the dimensions of these calibrated orifices. The small-conductance calibrated orifices between each pump and chamber also serve to minimize the effects of variations in pump speed.

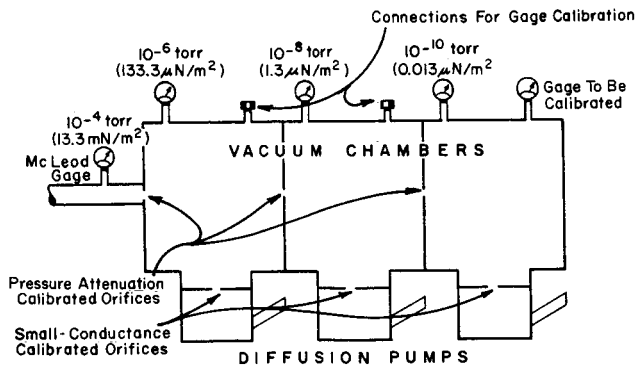


FIGURE 19. ULTRAHIGH-VACUUM CALIBRATION SYSTEM

The starting low pressure of the vacuum series is measured with a standard McLeod gage, which can measure down to 10^{-4} torr ($1.3 \times 10^{-2} \text{ N/m}^2$). The last of three pressure chambers will have 10^{-6} times the pressure measured by the McLeod gage; therefore the system can measure down to 10^{-10} torr ($0.013 \mu\text{N/m}^2$). This vacuum range is not dependent upon gas composition and temperature as long as there

are no large temperature variations from point to point in the system. Errors in the orifice technique, due to leaks or to outgassing from the walls, are overcome by high mass flowrates and bakeout in the high-vacuum region. Thus, this multistage method depends mainly on the geometric dimensions of pressure attenuation orifices and the standard pressure reading, provided that a specified minimum pumping speed is maintained.

IX. INSTRUMENTATION FOR MEASUREMENT OF OTHER EXTREME VALUES

In addition to ultrahigh vacuum, instrumentation for measurement of extreme values includes the measurement of very low water-vapor content in pressurizing gases, and the development, testing, and calibration of load cells for very high forces.

Considerable in-house research has been conducted on dewpoint instruments. Consolidated Electrodynamics Corp. (not under contract) developed a "moisture monitor," which uses an electrolysis principle and Faraday's law to measure water vapor content of gases in amounts as low as one-half part per million.

Developmental work on high-capacity load cells has been going on for many years. Much of the work has been done by private industry with its own funds and through research contracts with government agencies. Suggestions and test data offered by MSFC added to the fund of knowledge and resulted in the production of load cells which are used for static test of S-ICT. To advance the state of the art, MSFC initiated a research contract with Fluidyne Engineering for the development of a 5-million-pound (22.24-MN) load cell only 4 in. (10.2 cm) high. Prototypes have been tested and improvements are being made.

MSFC prepared specifications for testing and calibrating high-capacity load cells. Using these specifications, Gilmore Industries designed and built a 5-million-pound (22.24-MN) load-cell calibrator, which is now in operation at MSFC. The equipment uses 225,000 kg (496,000 lb) of calibration masses or deadweights, with an accuracy of 0.003 percent. It uses hydraulic cylinders and load cells to calibrate up to 5-million pounds force (22.24 MN), with an accuracy of 0.02 percent. Any one of the calibration masses, or any combination of them, can be applied. This is an advantage over most of the other dead-weight calibrators, which apply calibration masses only in the sequence in which they are stacked.

X. AUTOMATIC CALIBRATION SYSTEMS

Automatic calibration systems constituted another field in which MSFC did a considerable amount of research and development. Fifteen years ago the pressure balance was developed in-house for accurate reference pressure, and it was found most useful for calibration of pressure gages. Figure 20 shows an automatic pressure calibration system with a pressure balance as the heart of the system. A rotating piston converts the pressure into force, which presses down one arm of an equal-arm balance. This force is balanced by weights on the other arm of the balance. The pressure is regulated by adding or releasing air with solenoid valves. The accuracy of this calibrating system is 0.05 percent.

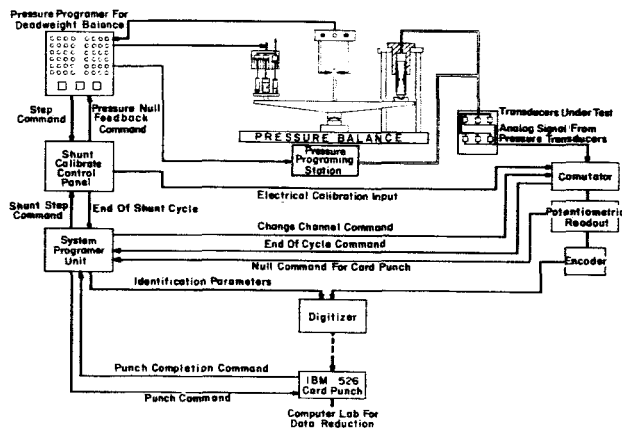


FIGURE 20. AUTOMATIC PRESSURE CALIBRATION SYSTEM

Under the impetus of expanding automation technology, MSFC initiated a research contract with Gilmore Industries for the automatic, laboratory-precision calibration of all pressure transducers on the Jupiter test stand, in which the pressure balance was used as a standard to obtain standard laboratory precision. Gilmore Industries proceeded to develop an automatic weight-handler for the pressure balance, and adapted a paper-tape programming device for automatic initiation and control of all the steps in pressure calibration. In this system, one group of transducers with the same pressure range are connected from the missile to the pressure balance by way of solenoid valves and manifolds. The appropriate weight increment for the pressure in the programmed step calibration is applied, and the pressure balance

is made to regulate the pressure. The transducer output then is recorded. Weights for the next pressure step are applied, and so on, until the calibration of the group of transducers is completed. The calibrated transducers are reconnected to the missile, and another group of transducers is connected to the pressure balance. The procedure is repeated until all the transducers are calibrated. A tape can be punched for any calibration program desired, so that calibration is fully automatic after a start button is pushed.

End-to-end calibration at the test stand is being replaced by shunt calibration. The resistance of shunt resistors is determined in the laboratory as a measure of pressure; then, instead of calibrating pressures directly at the test stand, an electrical calibration is made there with the shunt resistors.

As a result of this calibration work, the work load of the Instrument Laboratory has increased greatly. Consequently, automation in the laboratory and the use of computers for the tremendous data processing requirements have increased in importance. A computerized calibration system, developed to fulfill this need, is illustrated in Figure 20. The pressure transducers are in a heat chamber so that calibrations can be made at different temperatures. There may be up to 48 transducers in the chamber at one time. The pressure balance regulates the pressure, a digitizer conditions the signals of the pressure transducers, and an IBM card-puncher records the results on cards.

Other automatic calibration systems used by the laboratory are:

- a. An automatic thermocouple calibrator which compares up to 12 thermocouples with an NBS-calibrated standard thermocouple in a temperature-controlled oven. The power supply to the oven is regulated by an electronic unit, and the outputs of the thermocouples are automatically printed after each step of temperature has been reached.
- b. An automatic Mueller Bridge which balances automatically and prints the output of up to 12 resistance thermometers.
- c. An automatic load cell calibration system which increases or decreases the force of a hydraulic jack until the output of a standard load cell is equal to an electric signal preset by a step switch. This system is for test stand application.

SOUND SUPPRESSION TECHNOLOGY RESEARCH AT MARSHALL SPACE FLIGHT CENTER

By

Fritz Kramer

SUMMARY

This report describes some of the development tests conducted at Marshall Space Flight Center on sound suppressor models. These devices are designed to reduce the sound radiated into the atmosphere from the exhaust jets of large rocket engines. From theoretical considerations, the overall sound reduction capability of the tested models was expected to amount to 40 decibels. However, residual sound, radiated from the rocket engine and its installation, limited the attainable overall suppression to 24 decibels. Suppression of very low sound frequencies remains a special area of endeavor in future investigations.

The models were designed to be self-contained. They proved to possess very good operational characteristics.

I. INTRODUCTION

The high-intensity sound generated by high-thrust rocket engines has been of great concern to Marshall Space Flight Center (MSFC) and particularly to Test Laboratory. Sound powers of tens of millions of acoustical watts from rocket engines installed in the booster stage of the Saturn V moon rocket had been predicted as early as 1960, when the booster stage was under development. Sound powers of smaller magnitude, generated during static testing of less powerful missiles, already had caused concern in the population of nearby residential areas. Focusing of sound rays under particular atmospheric conditions also was known to affect areas at great distances from the test site. Therefore, Test Laboratory was obligated to study means to alleviate or eliminate these acoustic effects. The program which was established for this purpose later developed into two main activities, sound prediction and sound suppression.

In sound prediction, existing meteorological conditions are evaluated and correlated with the

sound power and the directional characteristics of the sound source. The magnitude of sound pressures expected in the area surrounding the test site is then determined through special computer programs. If meteorological conditions are unfavorable and too high a pressure level is predicted, the testing may have to be delayed or postponed. Sound prediction, therefore, is an operational activity, connected closely and directly with the test activity proper. It has to be performed for each test firing.

The purpose of sound suppression is to prevent the acoustic power from being generated, or from being radiated into the atmosphere. This requires a facility addition which may constitute a major investment. However, the sound suppressor, if designed as a self-contained unit, requires no operational procedures or personnel; it eliminates severe acoustic effects, and permits test firings at any time.

This report deals only with the sound suppression technology investigated at MSFC's Test Laboratory.

II. EARLY MODEL TESTS

The first tests conducted in 1960 and the following years may be considered today as exploratory from various points of view. Acoustic scaling laws were not well known, acoustic measuring and evaluation instrumentation was not well suited for field activities, and the mechanism underlying sound suppression was practically unknown. In addition, the sound sources, small liquid-propellant rocket engines, were inadequate acoustic models of the large powerplants. The power spectrum and kinetic energy of their exhaust jets did not properly simulate those of the large rocket engines. Also, there was no precedent for the design of rocket-engine sound suppressors. There was, therefore, little basis from which to start or extend. Most of the early models conceived and tested were either designed intuitively or along the lines of jet-engine devices. They employed baffles, perforated sheets, water sprays, and deflecting ducts to decelerate the rocket

exhaust gases and to spread them over a larger exit area, thus reducing the power of the generated sound.

Sound suppression obtained with some of these devices was encouraging: suppression of 19 decibels was obtained with a "diffuser cone," and 12 and 14 decibels with other devices. The sound source for these tests was a LOX-JP4 rocket engine with a thrust of 11.6 kN (2600 lb). When the system dimensions and other parameters of these devices were extrapolated to the size of the prototype for the Saturn V booster stage, however, serious technical shortcomings became apparent.

The difficulties with sound suppressors for rocket engines arise basically from the high temperature of the rocket exhaust and from the heat of recompression when the velocity of the jet is reduced. The exhaust gases have a temperature of about 1900°K (3000° F), and they leave the rocket exhaust nozzle with a velocity corresponding to a Mach number of 3.2 to 3.4. Although some exhaust gas at the periphery of the jet mixes immediately with air and reduces the temperature and velocity of this diffusion zone, the core of the jet remains unaffected for quite some distance (Fig. 1 and 2). Any obstacle placed into this supersonic stream causes formation of shock

waves with an increase in temperature due to this recompression. The increase in temperature across a plane shock wave is given by the temperature ratio:

$$\frac{T_1}{T} = \frac{1}{M^2} \left[1 + \frac{2k}{k+1} (M^2 - 1) \right] \left[1 + \frac{k-1}{k+1} (M^2 - 1) \right], \quad (1)$$

in which T and T₁ are the temperatures in front of and behind the shock wave, respectively; M is the Mach number in front of the shock; and k is the ratio of specific heats of gas. Typical values of M and T₁ are given in Table I, for k = 1.20 and T = 1745°K (3000° R). It is evident that the structural material

TABLE I. GAS TEMPERATURE BEHIND SHOCK WAVE

Mach Number	°K	T ₁ (°R)
2	2280	(4100)
2.5	2640	(4750)
3	3110	(5600)
3.5	3670	(6600)

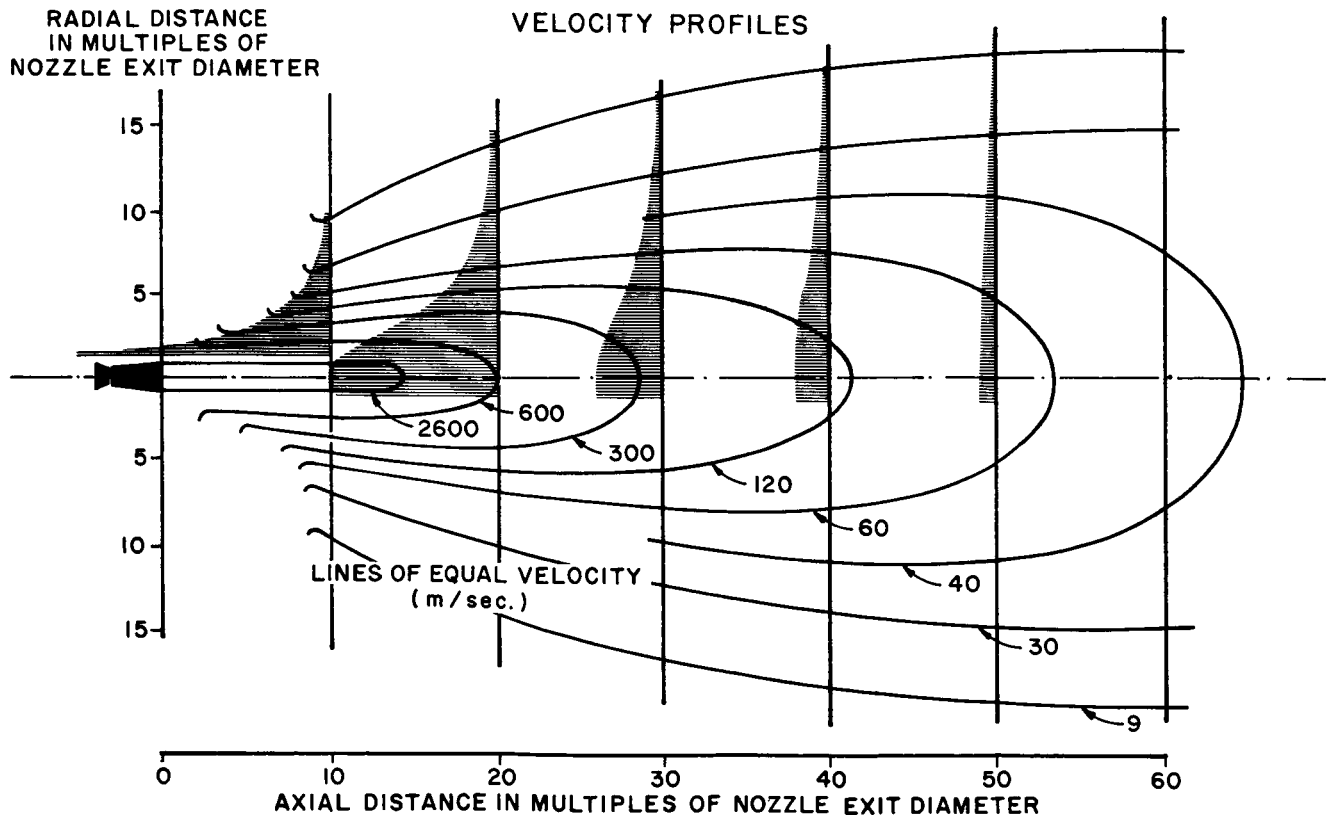


FIGURE 1. VELOCITY DISTRIBUTION IN ROCKET EXHAUST AT SEA LEVEL

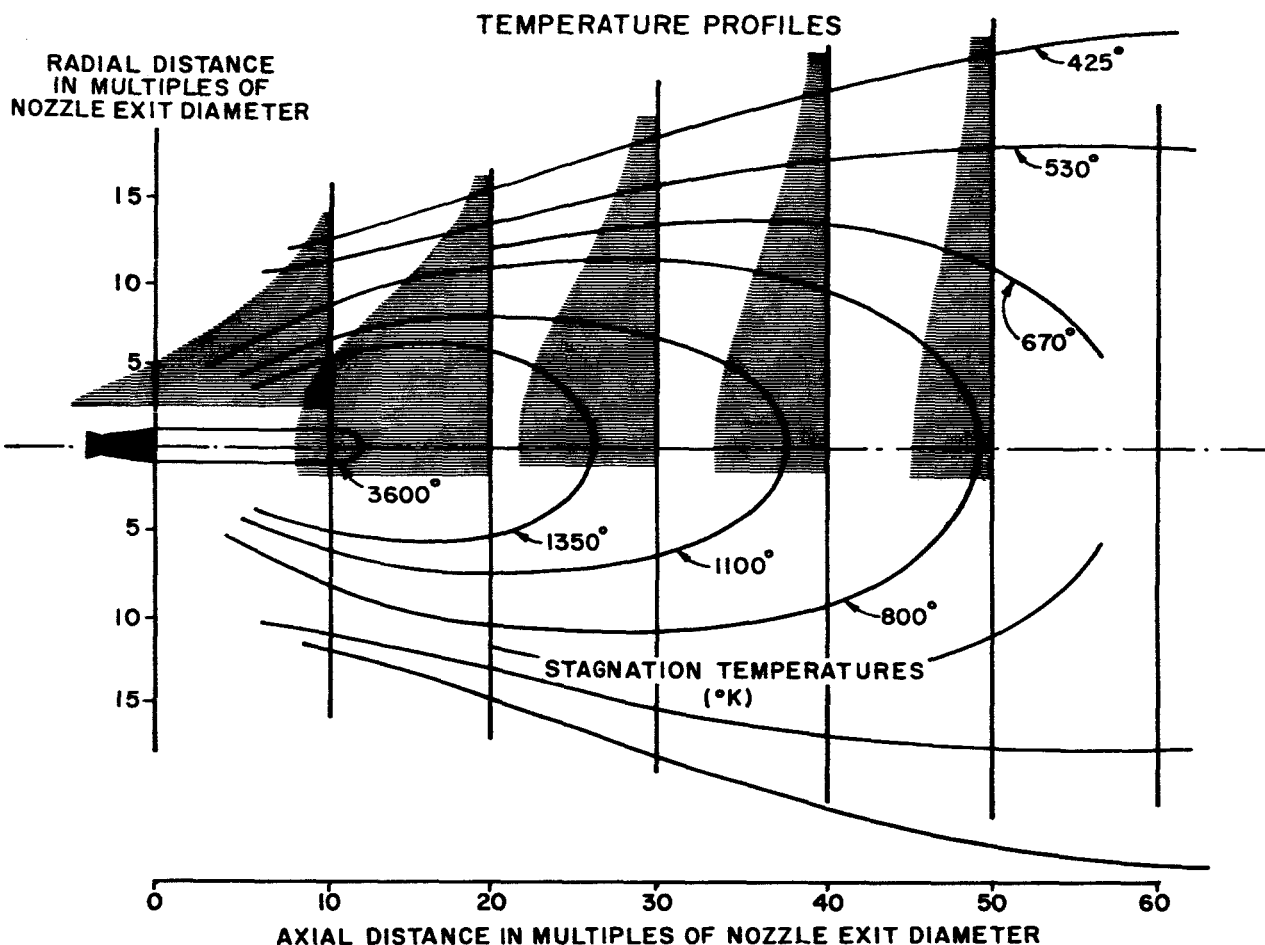


FIGURE 2. TEMPERATURE DISTRIBUTION IN ROCKET EXHAUST AT SEA LEVEL

of the sound suppressor, exposed to these temperatures, has to be cooled effectively to preserve its strength and structural integrity.

In the model tests, this cooling could be accomplished relatively easily by spraying water directly at these members. The amount of water needed ranged from $n = 2.0$ to $n = 5.4$, n being the weight ratio of cooling water flow rate to engine propellant flow rate. For a propellant flow rate of 7.5 kg/sec, the absolute flow rate of cooling water thus ranged from 0.015 to 0.04 m^3 (15 to 40 liters) per second. However, the propellant flow rate for the rocket engines of the Saturn V booster stage is 13 600 kg/sec (30 000 lb/sec). The water flow rate for cooling a sound suppressor based on these model types, therefore, would have to be from a minimum of 27 m^3 /sec to a possible maximum of 73 m^3 /sec. These flow rates would call for extremely large pumping stations with power requirements from 11.2 to 33.6 MW. The cost for such pumping stations with their associated equipment of valves, pipelines, and storage tanks would be prohibitive. A sound suppressor based on the design criteria developed in these early model tests was, therefore, not feasible.

In another approach, the rocket engine was fired into a sizable body of water. This method eliminated the cooling problem mentioned above, and accomplished an overall sound power reduction of 30 decibels; however, it required the largest structure of all models tested. (The water pool would have to be about 370 meters long and 170 meters wide for a Saturn V sound suppressor.) Also, explosions of propellants in the gaseous phase occurred from time to time, and the water mass was agitated so severely by the impinging jet that this method was not considered to be a practical solution to the sound suppressor design problem.

III. LATER TEST SERIES (1962 THROUGH SUMMER 1965)

By the summer of 1962, the continued studies on sound propagation and its effect on the surrounding areas had shown that the very low sound frequencies would require special attention because they are attenuated least by the atmosphere and can be felt strongly even as far as 15 kilometers from the test

site (Fig. 3). This fact created new requirements to be met by the sound suppressor: sound in the frequency range below 100 Hz was to be particularly well suppressed, and the threshold of annoyance of 110 decibels (ref 0.0002 microbar) was not to be reached in the populated areas surrounding a test site.

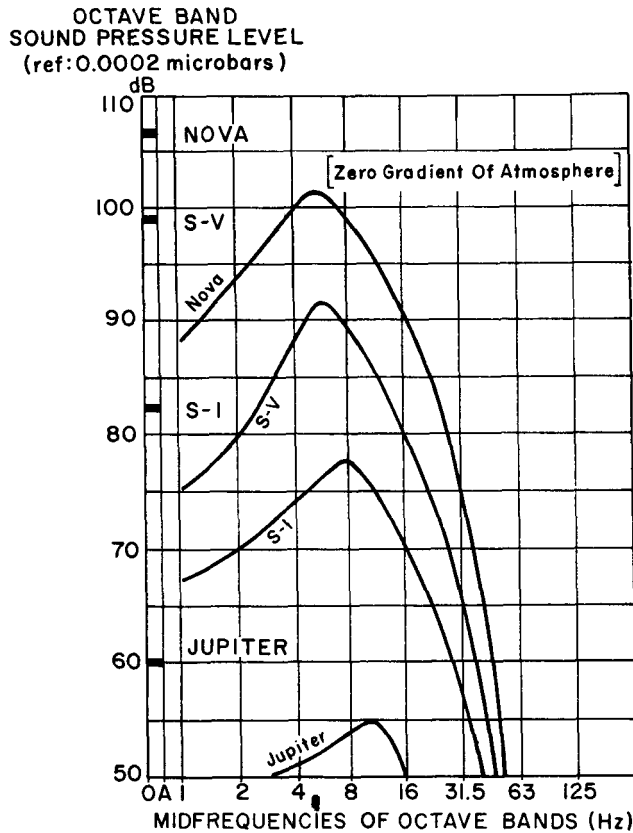


FIGURE 3. SOUND SPECTRA AT 15 KILOMETERS

The theory of Lighthill [1], that sound is generated aerodynamically, and that its power is proportional to the kinetic energy of the jet stream, contributed greatly to a basic understanding of the mechanism of sound suppression. The effectiveness of various designs now can be interpreted more easily in terms of gas exit velocity.

Figure 4 shows the relationship between sound power level of rockets and jet engines as a function of exhaust velocity. According to these test results, the sound power varies very closely with the sixth power of the exit velocity, if all other parameters remain constant. This relationship can be derived theoretically by expressing the kinetic energy $1/2mV^2$ in terms of the propellant flow rate and the exit area. The sound power (L_w) is obtained as

$$L_w = C_1 \frac{1}{g} \left(\frac{\dot{W}_p}{A_e} \right)^2 \cdot A_e \cdot v_e^6 \quad (2)$$

In this equation, \dot{W}_p is the propellant weight flow rate, A_e is the exit cross-sectional area, and v_e is the gas exit velocity. This relationship leads to the conclusion that good sound suppression is basically identical with good velocity reduction before the exhaust gases are admitted to the open atmosphere.

In the models built in 1962, the large reduction of the gas velocity was obtained by adding a large amount of water to the exhaust gas within an ejector-diffuser arrangement, commonly known as a jet pump. The exhaust gas constitutes the primary fluid; the water is the secondary fluid, which is pumped in large quantities without any additional power requirements. Within the diffuser, the momentum exchange between the jet and the water reduces the gas velocity, according to the law of conservation of momentum, to a velocity which is given by the equation

$$v = v_e \frac{1}{1+n} \quad (3)$$

In the equation, v_e is the exit velocity of the rocket jet, and n is the mass ratio of water flow rate to gas flow rate. This simple equation is obtained by disregarding the entrance velocity of the water into the diffuser or by assuming it to be negligible.

The addition of mass to the jet is evidently very effective, yielding a ten-fold decrease in velocity for a mass ratio of nine. Figure 4 shows the effect of n on the exit velocity and on the corresponding sound power.

However, a sound power reduction as indicated in Figure 4 by the application of a certain n value is not possible. The relation in Figure 4 is true only if the velocity is the sole independent variable. This is true because the addition of water to the gas not only reduces the gas velocity from v_e to $v_e \cdot \frac{1}{1+n}$, but also increases the weight flow rate from \dot{W}_p to $\dot{W}_p \cdot (1+n)$. The effect of mass addition on the sound power is obtained by introducing both these changes (or effects) into equation (2). This yields

$$L_w = C_2 \frac{1}{g} \left(\frac{\dot{W}_p}{A_e} \right)^2 \cdot A_e \cdot v_e^6 \left(\frac{1}{1+n} \right)^4 \quad (4)$$

While the unsuppressed sound power is directly proportional to the sixth power of the original exit

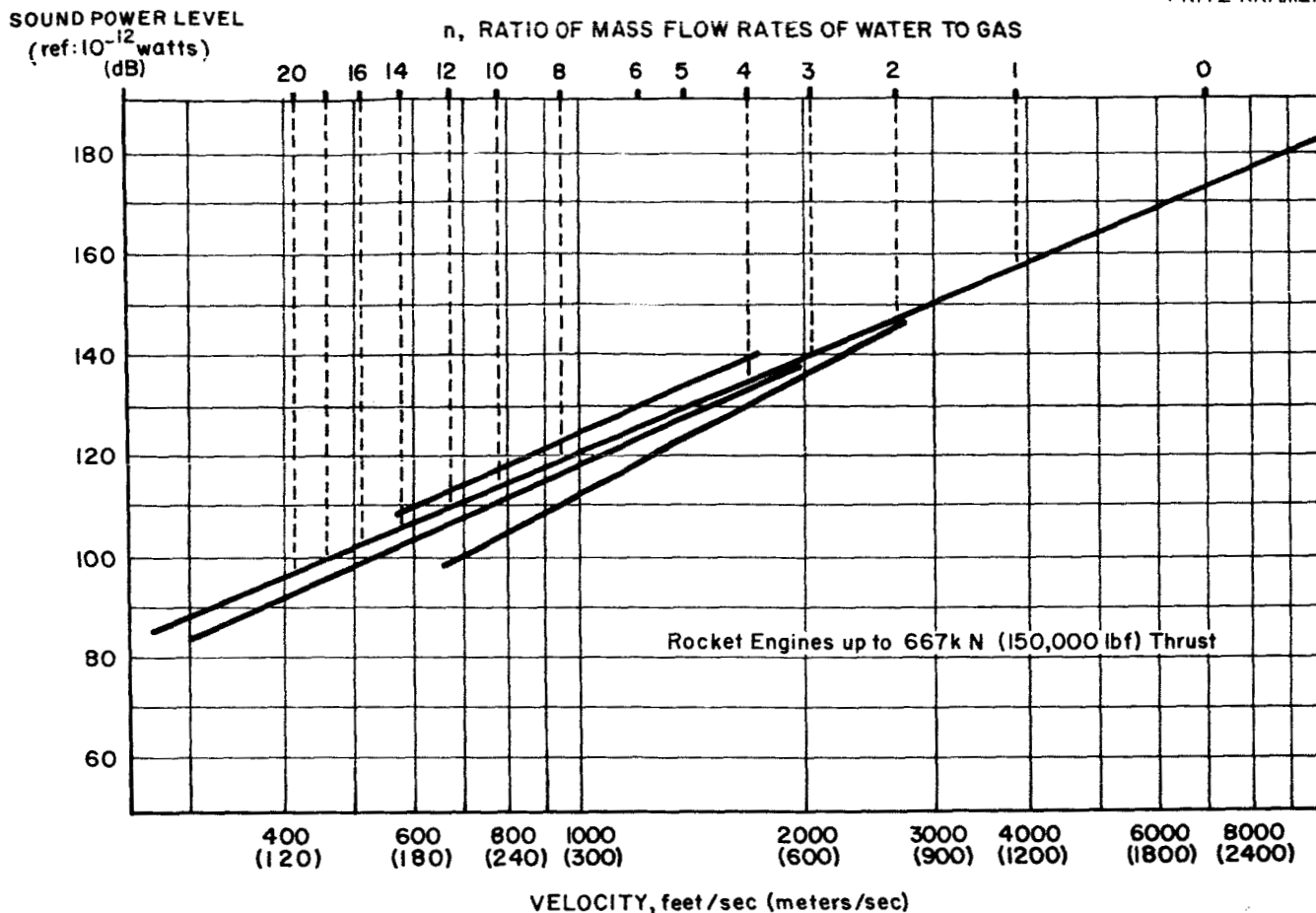


FIGURE 4. SOUND POWER LEVEL AS A FUNCTION OF EXHAUST VELOCITY

velocity v_e , the reduced power is inversely proportional to only the fourth power of the mass addition factor $(1 + n)$. Therefore, a sound power reduction of 40 decibels could be obtained theoretically for an n -value of 9 (or $1 + n = 10$) if all the water would take part in the momentum exchange, and if the gas emerging from the sound suppressor were the only remaining sound source. This, however, is not the case. Only a certain percentage (η) of the added water acts to reduce the gas velocity; therefore, the term $(1 + n)$ in equations (3) and (4) has to be replaced by the term $(1 + \eta \cdot n)$. Also, the rocket engine itself, the portion of its jet which is exposed to the atmosphere before entering the sound suppressor, and the structure of the sound suppressor, all emit some residual sound. The overall sound power of the installation, therefore, is the total emitted from all sources.

The residual sound power radiated from the powerplant, from its exposed jet, and from the sound suppressor structure may amount to only 1 percent of the initial acoustic power L_w , while the remaining 99 percent may be reduced by the sound suppressor

by a factor of $(1/10)^4$ to a value of $0.99 \cdot 10^{-4}$ as obtained for $1/(1 + n)^4$ for $n = 9$. The total sound power still in existence amounts then to

$$\left(\frac{1}{100} + \frac{99}{100} \cdot 10^{-4} \right) L_w = 0.010099 L_w \cong \frac{1}{10^2} \cdot L_w \quad (5)$$

With reference to the original sound power L_w , the new or suppressed sound power level is expressed as:

$$L_{w \text{ dB}} = 10 \cdot \log \frac{\frac{1}{10^2} L_w}{L_w} = 10 \cdot \log \frac{1}{10^2} = -20 \text{ dB.} \quad (6)$$

This means that the new sound power level is 20 decibels lower than the original one.

This example shows that the residual sound power radiating primarily from the rocket engine(s) and the short length of the free jet(s) actually determine the overall suppression performance of the

sound suppressor. The power level of the residual power, which determines the maximum suppression obtainable, is given in Table II.

TABLE II. MAXIMUM SOUND SUPPRESSION OBTAINABLE AS A FUNCTION OF THE RESIDUAL SOUND POWER

Residual power	Max. suppression
ΔL_w	ΔL_w^*
(%)	(dB)
1	-20
1/2	-23
1/4	-26
1/6	-28
1/8	-29
1/10	-30

*) ref 100% L_w

The overall sound suppression attained with the models (and later with the H-1 sound suppressor) was generally on the order of 21 to 24 decibels, regardless of the amount of additive water. Therefore, it can be concluded from Table II that the residual sound power in those models has been about 1 to 0.5 or 0.25 percent of the original sound power. Any future improvement in overall sound power reduction has to be accomplished through a reduction of this residual power by at least one order of magnitude. This probably will entail an enclosure around the rocket engine and its jet, which is objectionable from the test engineer's point of view. Unless some other means can be devised to contain the residual sound, it will be difficult to improve the overall sound suppression beyond the 24-decibel reduction obtained so far.

IV. INTERMEDIATE PROTOTYPE H-1

The model tests in 1962 initially employed a LOX-JP4 rocket engine with a thrust of 11 500 N (2600 lb), and later of 17 800 N (4000 lb). The Saturn V booster stage has a thrust of 33.4 MN (7.5 million lb). It was not considered advisable to apply the results from these model tests to the Saturn V

sound suppressor, since no scaling law was known to be applicable to such an extreme difference in power. The scaling laws not only have to pertain to the acoustical domain, but to the hydraulic, gas dynamic, and structural aspects as well.

It was decided, therefore, to build an intermediate-size prototype, using a surplus H-1 rocket engine with a thrust of 735 kN (165 000 lb). This thrust level requires a sound suppressor of a size halfway between the small models and the Saturn V prototype. The overall suppression obtained with this sound suppressor was 21 decibels for a water flow rate of 8 to 10 times the gas flow rate. The sound power spectrum is shown in Figure 5. This spectrum is flat, with a maximum suppression of 30 decibels at the 125-Hz octave midfrequency. At the lower frequencies, suppression is only 9 decibels at the 4-Hz midfrequency, an indication that the low sound frequencies are more difficult to suppress than the frequencies in the audible range.

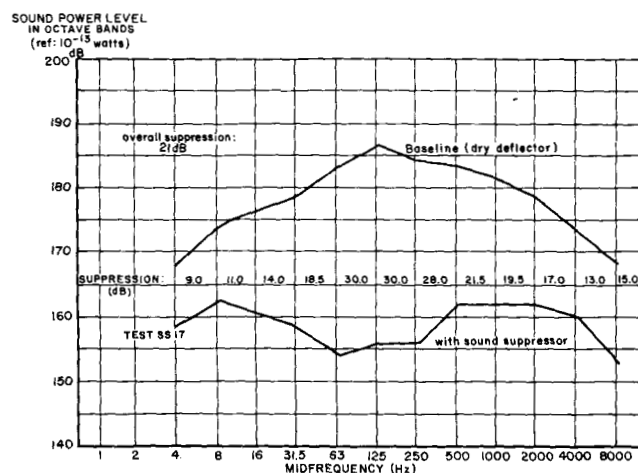


FIGURE 5. ACOUSTICAL PERFORMANCE OF SOUND-SUPPRESSION DEVICE

Except for the limited performance of the H-1 sound suppressor at the lower frequencies, the principle of mass addition in this intermediate prototype and in the small models has alleviated most or all of the previously existing problems. It has resolved the heating problem of the structure, it has solved the deceleration of the high-velocity, high-temperature jet within a very short distance and without the use of baffles or other obstacles, and it has completely eliminated the need for large pumping stations to provide the cooling water beyond that which is normally required for the operation of a test stand without a sound suppressor. In addition, the large flow rate of additive water for the Saturn V suppressor,

136 m³/sec (for $n = 10$), is induced to flow almost immediately upon engine ignition without operational procedure or personnel. Full flow is established within 2 to 3 seconds, and the flow ceases within a like time interval upon engine cutoff. This concept of operational simplicity has always been a part of the development and test program, and remains the final goal for a feasible sound suppression system.

V. MODELS OF SATURN V DESIGN

The improvement of the H-1 sound suppressor in the low-frequency range was one objective in later tests. Other areas of interest were the decreasing efficiency of the jet pump with increasing model size, the water transport capability of the exhaust-steam mixture, thermodynamic properties of the gas-steam-air mixture, and the separation of the water component from the gas-steam mixture before the latter leaves the sound suppressor. Although these last areas are important for the proper operation and function of the sound suppressor, the acoustical performance remained the prime objective in all tests. The solution to these many problems was approached through tests with models of the Saturn V design.

A small model (1:20 scale), with five engines of 17.9 kN (4000 lb) thrust each, was used to study the acoustical and gas dynamics characteristics only. The small scale for this model was permissible, since gas flow scales properly (except for viscous effects) if the linear scale is selected as the square root of the mass flow, with the gas velocity being the same in the model and in the prototype. Since gas velocity is identical in model and prototype, the acoustical performance should be identical also. This is true because for dynamically similar systems the sound pressure spectra measured at similar positions are the same when measured in constant percentage frequency bands, and when frequency is scaled inversely proportional to the scale factor. The total acoustic power is, of course, proportional to the thrust.

The sound power spectrum obtained with this model is shown in Figure 6. It is noteworthy that the overall sound suppression is again 21 decibels, as observed in previous models, but that suppression at the lower frequencies is now 17 decibels at 2 and 4 Hz, and even 24 decibels at 8-Hz midfrequency of the octave band. Water flow rate corresponded to $n = 8$.

According to the acoustic scaling laws, the 2, 4, and 8-Hz frequencies will shift to below 1 Hz in the prototype, and their power levels should increase by 26 decibels. It is believed that the reduction of the low frequency sound power in this model was obtained through the use of resonators. There remains some doubt, however, as to their effectiveness, since the performance in this low frequency area was not repeatable.

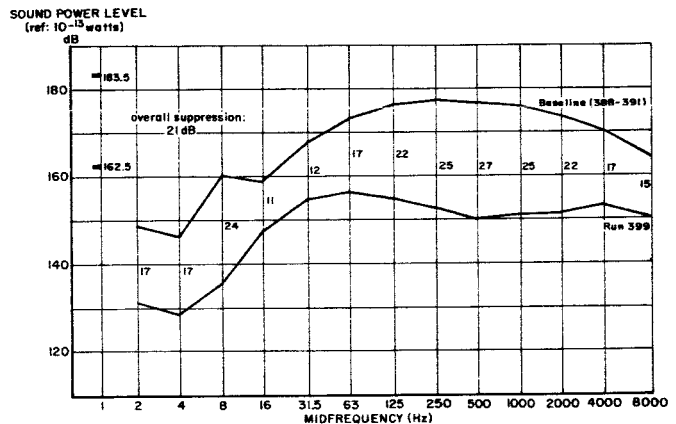


FIGURE 6. ACOUSTICAL PERFORMANCE OF A SOUND-SUPPRESSOR MODEL

Additional problems remaining in the operational area were studied with the H-1 sound suppressor, which was modified into a large model of the Saturn V suppressor design. The H-1 engine was replaced by a cluster of five rocket engines of 133 000 N (30 000 lb) thrust each, and the flat deflector used previously was replaced by a scale model of the deflector in the Saturn V test tower. The test objectives, mentioned above, scale according to Froude's model law. Additive water at mass ratio corresponding to $n = 18$ was necessary to meet all test objectives, such as the jet pump performance, water transport capability, and water separation. The theoretically possible sound power attenuation through resonators in the low-frequency range could not be verified by the acoustical measurements taken during these tests. It appears that this area deserves further study and research.

Figure 7 shows the sound power spectrum of the modified H-1 sound suppressor using the five-engine cluster (test SS 93) in comparison with the original model using the H-1 engine (test SS 17).

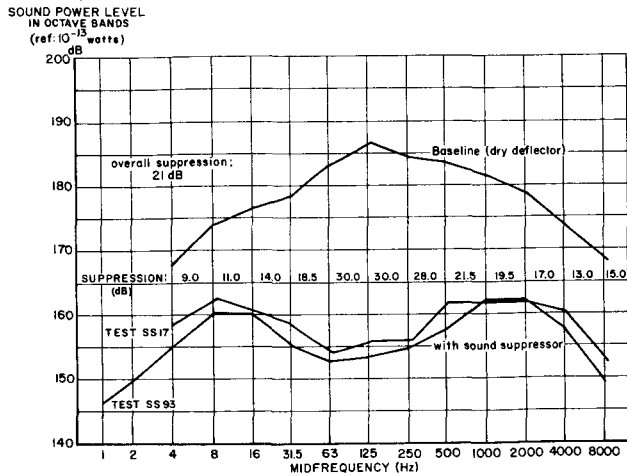


FIGURE 7. COMPARISON OF ACOUSTICAL PERFORMANCE OF TWO SOUND SUPPRESSORS

VI. CONCLUSIONS

The program was terminated in mid-1965, because at that time these basic objectives for a practical application had been accomplished:

1. The program had furnished a good basis for the design of a large sound suppressor for the Saturn V class booster stage.
2. It had met the requirement to sufficiently suppress the low-frequency sound so that certain criteria values of sound pressure level would not be exceeded.

Besides the above results for the practical application to the sound suppressor design, the following general and basic results have been obtained:

1. The basic mechanism in the reduction of the sound generated by rocket engines must be seen in the drastic reduction of the velocity of the exhaust jet before it can act on the still atmosphere and generate the sound through shear and turbulence.

2. The high temperature and velocity of the rocket exhaust defies the common approach to decelerate the gases through mechanical means, except in small units for which sufficient cooling water can be provided. For large rocket engines, the necessary flow rates of cooling water become excessive and prohibitively uneconomical.
3. The introduction of the jet pump, operated by the rocket jet as the driving fluid, solved both the problem of keeping the structure cool and of decelerating the exhaust jet effectively. It also allows for the design of a completely self-contained unit with no requirements for valves, auxiliary power, or operating personnel.
4. Attainable sound power level is equal to the sum of the residual sound power from various sources. These are: sound radiated from the rocket engine proper, sound generated by the part of the jet still exposed to the atmosphere before entering the sound suppressor, sound transmitted through the sound suppressor structure and its gas duct, and the sound generated by the escaping gas-steam mixture. The latter is considered immaterial compared with the other sound components.
5. Further reduction of the residual sound power is considered possible only through enclosing the free part of the rocket exhaust jet and the engine itself.
6. The suppression of low-frequency sound needs further study and experimentation. Present difficulty in obtaining greater suppression may be traced to the fact that the physical extension of structural members involved in the attenuation of the low-frequency sound is small compared with the wave length of the low-frequency sound waves. In addition, the high power of rocket noise may introduce non-linear effects, not considered, for instance, in resonator theory and general attenuation mechanisms.

REFERENCE

1. Lighthill, M. J.: Jet Noise. AIAA Journal, vol 1, no. 7, 1963, pp. 1507-1516.

APPROVAL

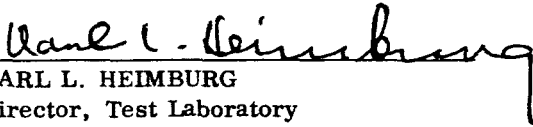
RESEARCH ACHIEVEMENTS REVIEW NO. 9

by

Gerhard H. R. Reisig, Albert E. Schuler, and Fritz Kramer

The information in this report has been reviewed for security classification. Review of any information concerning Department of Defense or Atomic Energy Commission programs has been made by the MSFC Security Classification Officer. This report, in its entirety, has been determined to be unclassified.

This document has also been reviewed and approved for technical accuracy.



KARL L. HEIMBURG
Director, Test Laboratory

DISTRIBUTION

MSFC INTERNAL

DIR	1
DEP-T	1
DEP-A	1
AST-P	1
CC	1
CC-P	1
LR	1
MA-S	1
PA	2
E-DIR	6
F& D-CH	1
R-DIR	3
R-S	1
R-TS	1
R-AS	5
R-AERO (Through Branch Level)	30
R-AERO-T	9
R-ASTR	25
R-EO-R (Reserve)	50
R-COMP (Through Branch Level)	10
R-COMP-T	5
R-ME (Through Branch Level)	21
R-RP (Through Branch Level)	8
R-P& VE (Through Branch Level)	79
R-QUAL (Through Branch Level);	26
R-QUAL-T	8
R-TEST (Through Branch Level)	12

DISTRIBUTION (Continued)

MSFC INTERNAL (Cont'd)

LVO	2
I-DIR	1
I-I/IB-MGR (Through Branch Level)	10
I-V-MGR (Through Branch Level)	10
I-E-MGR	3
I-MICH-MGR	20
I-MT-MGR	2
MS-T	25
MS-IP	2
MS-IL	8
MS-I, Daniel Wise	1
Air Force Space Systems Division Huntsville, Alabama	1

NASA HEADQUARTERS

Dr. Mac C. Adams, Code R, Washington, D. C.	1
Mr. Milton B. Ames, Jr., Code RV, Washington, D. C.	1
Mr. Walter Beckwith, Code MTP, Washington, D. C.	1
Dr. Raymond L. Bisplinghoff, Code A, Washington, D. C.	1
Mr. Edmond C. Buckley, Code T, Washington, D. C.	1
Mr. Oliver Bungardner, Code MLT, Washington, D. C.	1
Mr. Roland H. Chase, Code RET, Washington, D. C.	1
Mr. Fred J. DeMeritte, Code RV-1, Washington, D. C.	1
Mr. Robert W. Dunning, Code RBA, Washington, D. C.	1
Dr. James B. Edson, Code R-1, Washington, D. C.	1
Mr. Albert J. Evans, Code RA, Washington, D. C.	1
Mr. Harold B. Finger, Code RN, Washington, D. C.	1
Mr. W. Foster, Code SM, Washington, D. C.	1
Mr. Robert Freitag, Code MC, Washington, D. C.	1
Mr. Edward Z. Gray, Code MT, Washington, D. C.	1
Dr. John Holloway, Code SC, Washington, D. C.	1
Maj. Gen. David M. Jones, Code MD-P, Washington, D. C.	1
Dr. Walton L. Jones, Code RB, Washington, D. C.	1
Dr. Hermann H. Kurzweg, Code RR, Washington, D. C.	1
Mr. William E. Lilly, Code MP, Washington, D. C.	1
Dr. Douglas R. Lord, Code MTS, Washington, D. C.	1
Mr. Ivan Mason, Code MAT, Washington, D. C.	1
Dr. George E. Mueller, Code M, Washington, D. C.	1

DISTRIBUTION (Continued)

NASA HEADQUARTERS (Cont'd)

Mr. Joseph L. Murphy, Code KR, Washington, D. C.	1
Mr. Boyd C. Myers, Code RD, Washington, D. C.	1
Dr. J. Naugle, Code SG, Washington, D. C.	1
Dr. Homer E. Newell, Code S, Washington, D. C.	1
Mr. E. O. Pearson, Jr., Code RV-1, Washington, D. C.	1
Maj. Gen. Samuel C. Phillips, Code MA, Washington, D. C.	1
Mr. Maurice J. Roffersperger, Code MTE, Washington, D. C.	1
Mr. Melvin G. Rosche, Code RV-2, Washington, D. C.	1
Mr. Charles T. D'Aiutolo, Code RV-1, Washington, D. C.	1
Mr. J. Warren Keller, Code RV-1, Washington, D. C.	1
Mr. J. L. Sloop, Code RC, Washington, D. C.	1
Mr. S. M. Smolensky, Code MCD, Washington, D. C.	1
Mr. Frank J. Sullivan, Code RE, Washington, D. C.	1
Mr. William B. Taylor, Code MT, Washington, D. C.	1
Dr. M. Tepper, Code SF, Washington, D. C.	1
Mr. Adelbert Tischler, Code RP, Washington, D. C.	1
Mr. Theofolus Tsacoumis, Code RET, Washington, D. C.	1
Mr. Gene A. Vacca, Code REI, Washington, D. C.	1
Dr. John M. Walker, Code RET, Washington, D. C.	1

CENTERS

Mr. H. Julian Allen, Director NASA, Ames Research Center Moffett Field, California 94035	2
Dr. Kurt H. Debus, Director NASA, John F. Kennedy Space Center Kennedy Space Center, Florida 32899	2
Mr. Paul F. Bikle, Director NASA, Flight Research Center P. O. Box 273 Edwards, California 93523	2
Dr. John Clark, Acting Director NASA, Goddard Space Flight Center Greenbelt, Maryland 20771	1
Dr. William H. Pickering, Director NASA, Jet Propulsion Laboratory 4800 Oak Grove Drive Pasadena, California 91103	2
Dr. Floyd L. Thompson, Director NASA, Langley Research Center Langley Station Hampton, Virginia 23365	2

DISTRIBUTION (Continued)

CENTERS (Cont'd)

Dr. Abe Silverstein, Director NASA, Lewis Research Center 21000 Brookpark Road Cleveland, Ohio 44135	2
Mr. Warren Gillespie Code EA 5 NASA, Manned Spacecraft Center Houston, Texas 77001	15
Mr. J. P. Claybourne, EDV-4 Chief, Future Studies Office NASA, John F. Kennedy Space Center Kennedy Space Center, Florida 32899	1
Dr. Winston E. Kock NASA, Electronics Research Center 575 Technology Square Cambridge, Massachusetts 02139	2
Mr. A. R. Lawrence Management Analysis NASA, Electronics Research Center 575 Technology Square Cambridge, Massachusetts 02139	25
Mr. John Boyd, Technical Assistant Office of Assistant Director for Astronautics NASA, Ames Research Center Moffett Field, California 94035	1
Mr. Chesley H. Looney, Jr., Ass't Chief Advanced Development Division NASA, Goddard Space Flight Center Greenbelt, Maryland 20771	1
Mr. James F. Connors, Chief Office of Research Plans and Programs NASA, Lewis Research Center 21000 Brookpark Road Cleveland, Ohio 44135	1
Mr. James E. Calkins Office of Research and Advanced Development NASA, Jet Propulsion Laboratory 4800 Oak Grove Drive Pasadena, California 91103	1
Mr. A. R. Raffaelli PR-2 NASA, John F. Kennedy Space Center Kennedy Space Center, Florida 32899	1

DISTRIBUTION (Continued)

CENTERS (Cont'd)

Dr. A. H. Knothe Code TEC NASA, John F. Kennedy Space Center Kennedy Space Center, Florida 32899	1
Mr. Robert Hinckley NASA, Electronics Research Center Room 323 B 575 Main Street Cambridge, Massachusetts 02139	1
Dr. William G. Melbourne Mail Stop 180-300 Jet Propulsion Laboratory 4800 Oak Grove Drive Pasadena, California 91103	1
Scientific and Technical Information Facility Attn: NASA Rep. (S-AK/ RKT) P. O. Box 33 College Park, Maryland 20740	25
Mr. H. M. Drake, Chief Advanced Planning Office NASA, Flight Research Center Edwards Air Force Base Edwards, California 93523	1

DEPARTMENT OF DEFENSE

Dr. William W. Carter Chief Scientist U. S. Army Missile Command Bldg. 5250 Redstone Arsenal, Alabama	1
Mr. John McDaniel Technical Director Research and Development Directorate U. S. Army Missile Command Bldg. 4505 Redstone Arsenal, Alabama	12
Lt. M. V. Vasilik Arnold Air Force Base Tullahoma, Tennessee 37389	30

DISTRIBUTION (Continued)

CONTRACTORS

The Boeing Company Attn: Mr. John Pehrson Huntsville Industrial Center Huntsville, Alabama	5
Brown Engineering Company, Inc. Mail Stop 5 300 Sparkman Drive, NW Huntsville, Alabama	5
Chrysler Corporation Attn: Mr. Howard Blood 1312 Meridian, North Huntsville, Alabama	5
Douglas Aircraft Holiday Office Center Huntsville, Alabama	5
General Electric Company Holiday Office Center Huntsville, Alabama	5
Mr. Robert A. Hardesty General Electric Company Ordnance Department 100 Plastics Avenue Room 1040 Pittsfield, Massachusetts 01201	5
Hayes International Corporation 204 Oakwood Avenue, NE Huntsville, Alabama	5
IBM Corporation 150 Sparkman Drive, NW Huntsville, Alabama	5
Lockheed Aircraft Corporation Holiday Office Center Huntsville, Alabama	5
North American Aviation, Inc. Holiday Office Center Huntsville, Alabama	5
Northrop Corporation Holiday Office Center Huntsville, Alabama	5
Mr. W. G. Calder General Electric Co. Suite 13 Holiday Office Center Huntsville, Alabama	1

DISTRIBUTION (Continued)

CONTRACTORS (Cont'd)

Sperry Rand Corporation 8110 Memorial Parkway, SW Huntsville, Alabama	5
Space Craft, Incorporated 8620 Memorial Parkway, SW Huntsville, Alabama	1
Spaco, Incorporated 3022 University Drive, NW Huntsville, Alabama	5
University of Alabama 4701 University Avenue, NW Huntsville, Alabama	5
Vitro Corporation of America Holiday Office Center Huntsville, Alabama	5
Wyle Laboratories Highway 20, West Huntsville, Alabama	5

UNIVERSITIES AND COLLEGES

Alabama A&M College Huntsville, Alabama	1
University of Alabama Tuscaloosa, Alabama	1
Dr. Clyde Hull Cantrell, Director Ralph Brown Draughon Library Auburn University Auburn, Alabama	4
University of California (UCLA) Los Angeles, California	1
Carnegie Institute of Technology Pittsburgh, Pennsylvania	1
Case Institute of Technology Cleveland, Ohio	1
Clemson University Clemson, South Carolina Attn: Mr. J. W. Gourlay	1

DISTRIBUTION (Continued)

UNIVERSITIES AND COLLEGES (Cont'd)

Mr. S. G. Nicholas Director of Engineering Research Clemson University Clemson, South Carolina	1
Columbia University New York, New York 10027	1
Librarian Columbia University Nevis Laboratories Irvington, New York 10533	1
University of Denver Denver, Colorado	1
Director's Office Denver Research Institute University of Denver Denver, Colorado	1
Department of Nuclear Engineering Sciences University of Florida Gainesville, Florida 32603	1
Mrs. J. Henley Crosland Director, Libraries Georgia Institute of Technology Atlanta, Georgia	9
University of Georgia Athens, Georgia	1
Louisiana State University Baton Rouge, Louisiana	1
Massachusetts Institute of Technology Cambridge, Massachusetts	1
University of Michigan Ann Arbor, Michigan	1
Mississippi State University State College, Mississippi	1
University of Mississippi University, Mississippi	1
University of North Carolina Chapel Hill, North Carolina	1

DISTRIBUTION (Continued)

UNIVERSITIES AND COLLEGES (Cont'd)

Northeast Louisiana College Monroe, Louisiana	1
Ohio State University Columbus, Ohio	1
Ohio University Athens, Ohio	1
Oklahoma State University Stillwater, Oklahoma	1
University of Pittsburgh Pittsburgh, Pennsylvania	1
Princeton University Princeton, New Jersey	1
Library School of Electrical Engineering Purdue University Lafayette, Indiana	1
Rev. R. J. Henle, S. J. Vice President for Academic Matters and Research Director Saint Louis Univeristy 221 N. Grand Blvd. St. Louis, Missouri	2
Stanford University Palo Alto, California	1
Syracuse University Syracuse, New York	1
University of Tennessee Knoxville, Tennessee	1
Cushing Memorial Library Texas A&M University College Station, Texas	1
Mr. Harry E. Whitmore, Head Space Technology Division Texas A&M University College Station, Texas	2
University of Texas Austin, Texas	1

DISTRIBUTION (Concluded)

UNIVERSITIES AND COLLEGES (Cont'd)

Science Librarian Tulane University Library New Orleans, Louisiana 70118	1
The Joint University Libraries 419-21st Avenue, South Nashville, Tennessee	1
Science Library Vanderbilt University Box 1521, Station B Nashville, Tennessee	1
Virginia Polytechnic Institute Blacksburg, Virginia	1
Washington State Pullman, Washington	1
Mr. H. W. Hsu Associate Professor of Chemical Engineering University of Tennessee Knoxville, Tennessee 37916	1
Professor F. N. Peebles Department of Engineering Mechanics University of Tennessee Knoxville, Tennessee	1
Mr. W. Byron Long Director of Special Projects Mississippi Research and Development Center P. O. Drawer 2470 Jackson, Mississippi	1
Engineering Library University of Arkansas Fayetteville, Arkansas	1

UNITS OF MEASURE

In a prepared statement presented on August 5, 1965, to the U. S. House of Representatives Science and Astronautics Committee (chaired by George P. Miller of California), the position of the National Aeronautics and Space Administration on Units of Measure was stated by Dr. Alfred J. Eggers, Deputy Associate Administrator, Office of Advanced Research and Technology:

"In January of this year NASA directed that the international system of units should be considered the preferred system of units, and should be employed by the research centers as the primary system in all reports and publications of a technical nature, except where such use would reduce the usefulness of the report to the primary recipients. During the conversion period the use of customary units in parentheses following the SI units is permissible, but the parenthetical usage of conventional units will be discontinued as soon as it is judged that the normal users of the reports would not be particularly inconvenienced by the exclusive use of SI units."

The International System of Units (SI Units) has been adopted by the U. S. National Bureau of Standards (see NBS Technical News Bulletin, Vol. 48, No. 4, April 1964).

The International System of Units is defined in NASA SP-7012, "The International System of Units, Physical Constants, and Conversion Factors," which is available from the U. S. Government Printing Office, Washington, D. C. 20402.

SI Units are used preferentially in this series of research reports in accordance with NASA policy and following the practice of the National Bureau of Standards.